Chapter 4

Buckling and Postbuckling Response of Hybrid Composite Plates under Uniaxial Compressive Loading

4.1. Introduction

This chapter deals with experimental and numerical study of postbuckling response and strength of functionally graded and sandwich hybrid composite plates under uniaxial compression. Carbon and glass fiber reinforced polymers (FRP's) were used in preparing the plain CFRP, plain GFRP, functionally graded hybrid (FH) and sandwich hybrid (SH) plates.

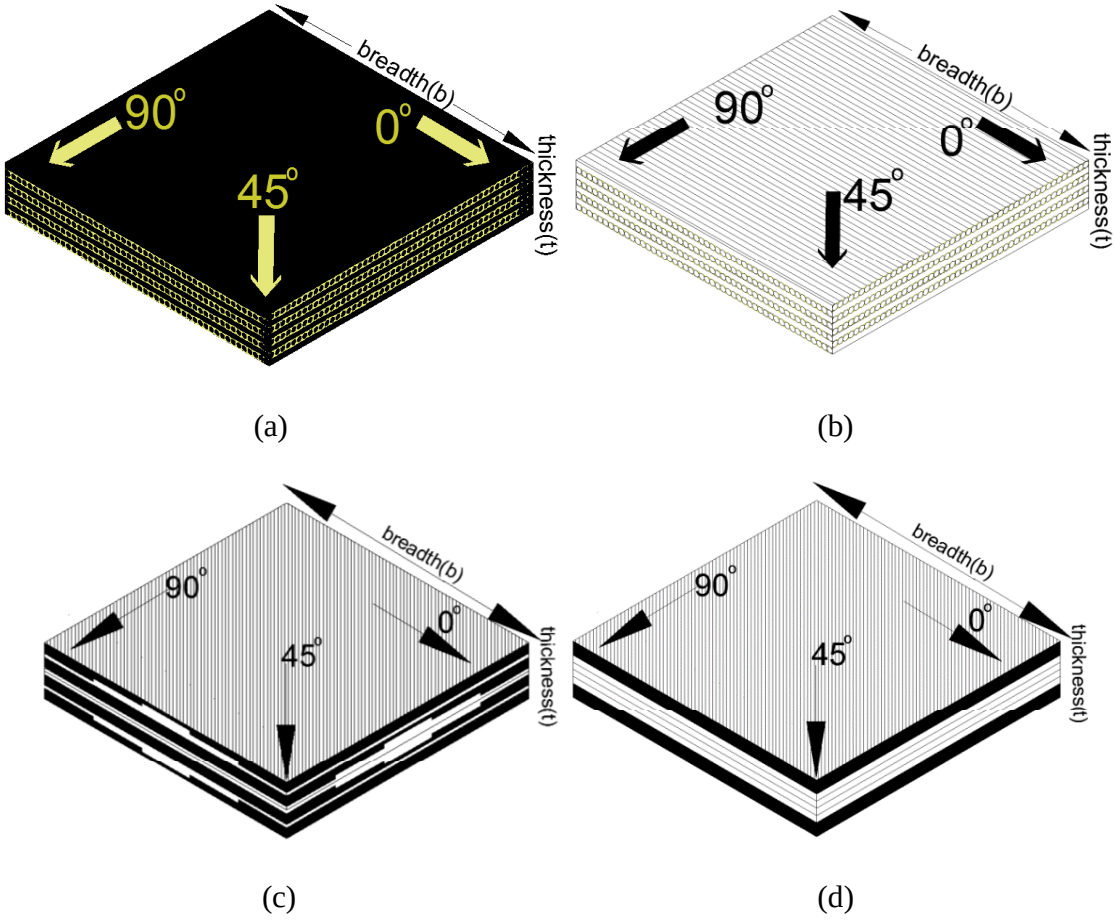

Fig. 4.1. Layup sequences of carbon surfaced hybrid laminates: (a) carbon fiber reinforced polymer (CFRP) laminate; (b) glass fiber reinforced polymer (GFRP) laminate; (c) Functionally graded hybrid (FH) laminate; (d) Sandwich hybrid (SH) laminate

Fiber volume fraction in all the plate was limited to 60% to eliminate the matrix dominant failure. Plain CFRP, plain GFRP, functionally graded hybrid, and sandwich hybrid layup sequences were fabricated and modeled as shown in Figure 4.1.

4.2. Experimental and numerical approaches

4.2.1. Experimental approach

Square plates of size 279x279x2.16mm were fabricated in the advance composite laboratory of civil engineering department, BITS Pilani using hand layup procedure which includes pressing of wet laminate between two heavy mild steel plates bolted together and oven cured. Later, the obtained hard thin plates were tested under the application of edge compressive loading at servo hydraulic loading frame testing facility. The boundary conditions considered are simply supported on all the four edges of the plate. Fiber orientation such as $(0/90)_{4s}$ is considered for the testing of plates. Fig. 4.1(a) depicts plain CFRP plate while Fig. 4.1(b) shows plain GFRP plate with fiber aligned in (0/90) directions. The directions of the fibers for a typical laminate are mentioned in Fig. 4.1. In case of functionally graded hybrid plate, 100% carbon fiber is dispersed in the top lamina then the second layer consists of 66% carbon fibers and 33% glass fibers, further the third layer consists of 33% carbon fibers and 66% glass fibers and at last the fourth layer consists of 100% glass fibers. This complete set of four layers makes one laminate with stacking sequence of $(0/90)_{4s}$ fiber direction as shown in Fig. 4.1(c). In sandwich hybrid composite plate, top and bottom layers are provided with carbon fibers and glass fibers are provided in the core as shown in Fig. 4.1(d). The plate thickness is maintained same (i.e. 2.16 mm) in all the plain FRP, FH, and SH plates. The plate was initially fixed in the apparatus with all edges simply supported as shown in Fig. 4.2(a). The load is applied axially through a specially designed test fixture on the top edge of the plate and four Linear Variable Differential Transformers (LVDT) are attached on the surface of the plate to measure lateral deflection of the plate under compression as depicted in Fig. 4.2(b). Rate of loading of the actuator at the servo hydraulic loading frame facility as shown in Fig. 4.2 (a) was calculated using Eq. (1) since buckling mode mainly depends on the rate of loading of the actuator.

$$R = \frac{Zb^2}{6t} \tag{1}$$

where, ‘R’ is the rate of cross head motion (mm/s), ‘Z’ is the rate of straining of the outer fiber (mm/mm/s) which is equal to 0.01, ‘b’ is the breadth of the plate (mm), and ‘t’ is the thickness of the plate (mm).

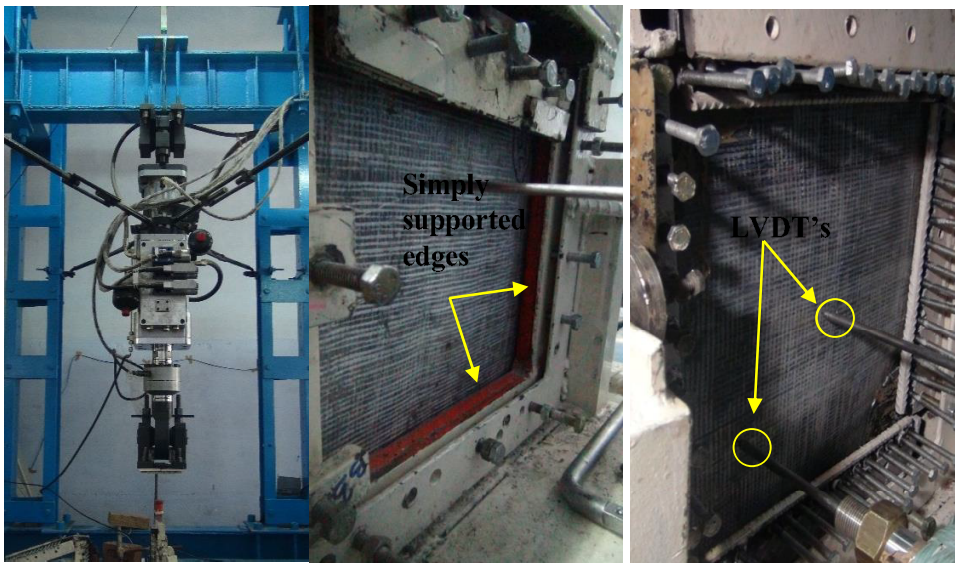

(a) (b) (c)

Fig. 4.2. Experimental setup of the composite plate: (a) Actuator Plate edges simply

Further load was applied on the composite plates until failure as shown in Fig. 4.3. Similar buckling can be seen in all the plates and the propagation of cracks started from the edges as shown in Fig. 4.3(g). This behavior was observed in case of plates analyzed numerically.

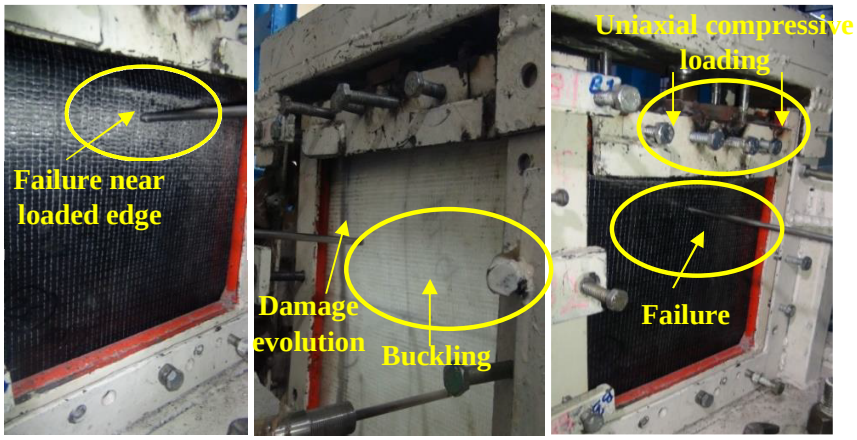

(a) (b) (c)

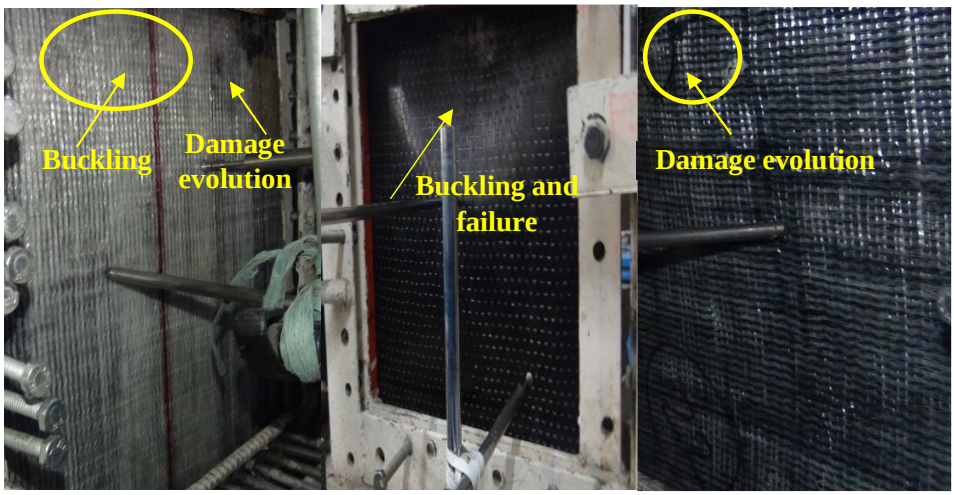

(d) (e) (f)

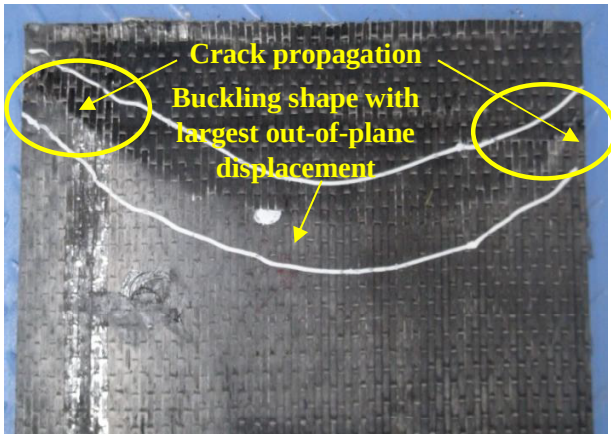

(g)

Fig. 4.3. Buckling analysis of composite laminates: (a) CF_0-90_NH; (b) GF_0-90_NH; (c) CG_0-90_FH (d) GC_0-90_FH; (e) CG_0-90_SH; (f) GC_0-90_SH; (g) Buckling shape and cracks

In Fig. 4.3(a), CF_0-90_NH represents non hybrid carbon fiber reinforced polymer plate with stacking sequence (0/90), GF_0-90_NH represents non hybrid glass fiber reinforced polymer plate with stacking sequence (0/90), CG_0-90_FH represents functionally graded hybrid (carbon fiber on surface and glass fiber in the core) fiber reinforced polymer plate with stacking sequence (0/90), GC_0-90_FH represents functionally graded hybrid (glass fiber on surface and carbon fiber in the core) fiber reinforced polymer plate with stacking sequence (0/90), CG_0-90_SH represents sandwich hybrid (carbon fibers on top layers and glass fibers in the middle layers) fiber reinforced polymer plate with stacking sequence (0/90), and GC_0-

90_SH represents sandwich hybrid (glass fibers on top layers and carbon fibers in the middle layers) fiber reinforced polymer plate with stacking sequence (0/90). The mechanical properties of these fibers used such as carbon fiber and glass fiber are given in Table 4.1.

Table 4.1. Material properties of the carbon and glass epoxy laminate

Mechanical properties	Carbon-Epoxy	Glass-Epoxy	Strength properties	Carbon-Epoxy	Glass-Epoxy
E_1	69.1GPa	24.3GPa	X_t	1150MPa	750MPa
$E_2=E_3$	5.46GPa	5.18GPa	X_c	840MPa	680MPa
$G_{12}=G_{13}$	2.73GPa	2.59GPa	Y_t	26MPa	74MPa
G_{23}	1.37GPa	1.29GPa	Y_c	36MPa	81MPa
υ_{12}	0.25	0.3	S=T	18MPa	40MPa

4.2.2. Numerical study

Finite element analysis-based software (ABAQUS) is used for simulating these plates for postbuckling analysis, response, and strength. Plates have been modeled with similar dimensions, as considered in experimental investigation.

Table 4.2. Nomenclature of the non-hybrid and hybrid composite plates without cutouts

Plate ID	Details
CF_0-90_NH	Non hybrid plain carbon fiber reinforced polymer plate aligned in $(0/90)_{4s}$ direction
GF_0-90_NH	Non hybrid plain glass fiber reinforced polymer plate aligned in $(0/90)_{4s}$ direction
CG_0-90_FH	Functionally graded hybrid plate with carbon fiber surfaced and glass fiber in the core aligned in $(0/90)_{4s}$ direction
GC_0-90_FH	Functionally graded hybrid plate with glass fiber surfaced and carbon fiber in the core aligned in $(0/90)_{4s}$ direction
CG_0-90_SH	Sandwich hybrid plate with carbon fiber in the top and glass fiber in the middle layers aligned in $(0/90)_{4s}$ direction

GC_0-90_SH	Sandwich hybrid plate with glass fiber in the top and carbon fiber in the middle layers aligned in $(0/90)_{4s}$ direction
CF_45-45_NH	Non hybrid plain carbon fiber reinforced polymer plate aligned in $(-45/+45)_{4s}$ direction
GF_45-45_NH	Non hybrid plain glass fiber reinforced polymer plate aligned in $(-45/+45)_{4s}$ direction
CG_45-45_FH	Functionally graded hybrid plate with carbon fiber surfaced and glass fiber in the core aligned in $(-45/+45)_{4s}$ direction
GC_45-45_FH	Functionally graded hybrid plate with glass fiber surfaced and carbon fiber in the core aligned in $(-45/+45)_{4s}$ direction
CG_45-45_SH	Sandwich hybrid plate with carbon fiber in the top and glass fiber in the middle layers aligned in $(-45/+45)_{4s}$ direction
GC_45-45_SH	Sandwich hybrid plate with glass fiber in the top and carbon fiber in the middle layers aligned in $(-45/+45)_{4s}$ direction
CF_QSI_NH	Non hybrid plain carbon fiber reinforced polymer plate aligned in $(-45/+45/0/90)_{2s}$ direction (quasi-isotropic sequence)
GF_QSI_NH	Non hybrid plain glass fiber reinforced polymer plate aligned in $(-45/+45/0/90)_{2s}$ direction
CG_QSI_FH	Functionally graded hybrid plate with carbon fiber surfaced and glass fiber in the core aligned in $(-45/+45/0/90)_{2s}$ direction
GC_QSI_FH	Functionally graded hybrid plate with glass fiber surfaced and carbon fiber in the core aligned in $(-45/+45/0/90)_{2s}$ direction
CG_QSI_SH	Sandwich hybrid plate with carbon fiber in the top and glass fiber in the middle layers aligned in $(-45/+45/0/90)_{2s}$ direction
GC_QSI_SH	Sandwich hybrid plate with glass fiber in the top and carbon fiber in the middle layers aligned in $(-45/+45/0/90)_{2s}$ direction

Nomenclature for plates without cutouts has been given in Table 4.2 while those with cutouts have been given in Table 4.3. Initial steps in the analysis include modeling of plate, assigning properties, load application and implying boundary conditions. In the initial step, buckling

option under linear perturbation procedure was implemented to determine the buckling load prior to postbuckling analysis. The buckling load obtained has been incorporated for non-linear analysis. Static-riks procedure has been employed for non-linear postbuckling analysis. Geometric imperfection of 0.0000001% has been considered after repeated iterations. Shell edge compressive loading in y-direction was applied on the plate and furthermore, meshing was done to the plate with an approximate element size of 0.004.

Table 4.3. Nomenclature of the functionally graded composite plates with cutouts

Plate ID	Details
CG_FH_C_(0/90)	Functionally graded hybrid (FH) plate with carbon fiber surfaced and glass fiber in the core aligned in $(0/90)_{4s}$ direction with circular shaped cutout
CG_FH_D_(0/90)	FH plate with carbon fiber in the top and glass fiber in the middle aligned in $(0/90)_{4s}$ direction with diamond shaped cutout
CG_FH_EH_(0/90)	FH plate with carbon fiber in the top and glass fiber in the middle aligned in $(0/90)_{4s}$ direction with ellipse shaped cutout aligned horizontally
CG_FH_EV_(0/90)	FH plate with carbon fiber in the top and glass fiber in the middle aligned in $(0/90)_{4s}$ direction with ellipse shaped cutout aligned vertically
CG_FH_S_(0/90)	FH plate with carbon fiber in the top and glass fiber in the middle aligned in $(0/90)_{4s}$ direction with square shaped cutout
CG_FH_C_(-45/+45)	FH plate with carbon fiber surfaced and glass fiber in the core aligned in $(-45/+45)_{4s}$ direction with circular shaped cutout
CG_FH_D_(-45/+45)	FH plate with carbon fiber in the top and glass fiber in the middle aligned in $(-45/+45)_{4s}$ direction with diamond shaped cutout

CG_FH_EH_(-45/+45)	FH plate with carbon fiber in the top and glass fiber in the middle aligned in $(-45/+45)_{4s}$ direction with ellipse shaped cutout aligned horizontally
CG_FH_EV_(-45/+45)	FH plate with carbon fiber in the top and glass fiber in the middle aligned in $(-45/+45)_{4s}$ direction with ellipse shaped cutout aligned vertically
CG_FH_S_(-45/+45)	FH plate with carbon fiber in the top and glass fiber in the middle aligned in $(-45/+45)_{4s}$ direction with square shaped cutout
CG_FH_C_(QSI)	FH plate with carbon fiber surfaced and glass fiber in the core aligned in $(-45/+45/0/90)_{2s}$ direction with circular shaped cutout
CG_FH_D_(QSI)	FH plate with carbon fiber in the top and glass fiber in the middle aligned in $(-45/+45/0/90)_{2s}$ direction with diamond shaped cutout
CG_FH_EH_(QSI)	FH plate with carbon fiber in the top and glass fiber in the middle aligned in $(-45/+45/0/90)_{2s}$ direction with ellipse shaped cutout aligned horizontally
CG_FH_EV_(QSI)	FH plate with carbon fiber in the top and glass fiber in the middle aligned in $(-45/+45/0/90)_{2s}$ direction with ellipse shaped cutout aligned vertically
CG_FH_S_(QSI)	FH plate with carbon fiber in the top and glass fiber in the middle aligned in $(-45/+45/0/90)_{2s}$ direction with square shaped cutout

Different mesh sizes were considered as shown in Fig. 4.4 and the corresponding buckling loads of a composite plate are determined. From Fig. 4.4, buckling loads got converged at 50x50 (no. of elements in u & v direction) which is relative to the element size of 0.004. The plate is modelled with four-noded linear shell elements (S4R) with reduced integration. Thereafter, Tsai-Hill failure criterion has been incorporated in the step module of non-linear buckling analysis for determining the first ply failure load which corresponds to first ply failure in a ply in the plate after the loading is applied. Ultimate failure load is marked at a point where

the plate is unable to take any further load as per the ABAQUS analysis. In ABAQUS numerical study, ultimate failure load is occured at a point where the plate becomes unstable. Geometrically nonlinear problems sometimes involve buckling or collapse behavior. Abaqus offers an automated version of the stabilization approach for the static analysis procedures. Unstable phase of the response can be found by using the modified riks method.

The Riks method can be used to solve postbuckling problems both with stable and unstable behaviours. To analyze a postbuckling problem, it must be turned into a problem with continuous response instead of bifurcation. This effect can be accomplished by introducing an

mode before the critical load is reached. This method is used for cases where the loading is proportional i.e., where the load magnitudes are governed by a single scalar parameter (load proportionality factor). This method can provide solutions even in cases of complex and unstable response.

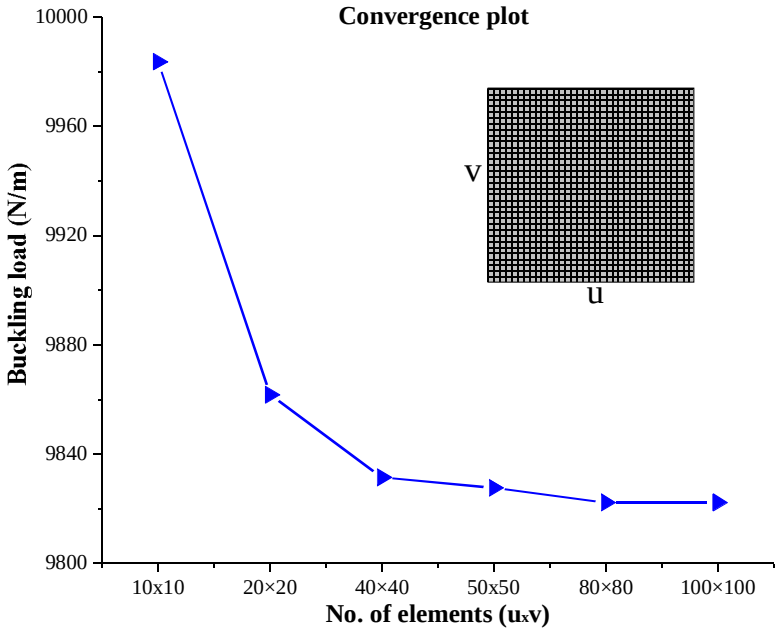

Fig. 4.4. Convergence plot of buckling load in carbon fiber reinforced composite plate aligned in (0/90) direction.

In case of problems with material non-linearity, geometric non-linearity prior to buckling or unstable postbuckling response, load-deflection riks analysis must be performed to investigate the problem further. To measure the progress of the solution, arc length quantity is used along the

static equilibrium path in load-displacement space. This arc length approach provides solution regardless stable or unstable response. The plate reaches the ultimate load carrying capacity at a specified degree of freedom where it reaches a maximum value of load proportionality factor or a maximum dispacement value. In the current research maximum load magnitude has been considered, further the plate becomes unstable and the drop in load begins.

4.3. Results & Discussion

4.3.1. Experimental study

The experimental tests were conducted on the plain CFRP, plain GFRP, functionally graded hybrid (FH), and sandwich hybrid (SH) plates aligned in (0/90) fiber direction. Initially, when the load was applied on the plate, resistance was offered by the plate without any out-of-plane displacement. Buckling of the composite plate occurs when the axial compression reaches a critical value called as buckling load. After reaching critical load, the plate started buckling i.e., plate got displaced in the direction normal to the plane of plate. The plies in the plate failed one after the other as they reach their maximum load carrying capacity. Damage occurred near/towards the loading point in all the plates as shown in Fig. 4.3. Initial failure started near the loading edge of the CF_0-90_NH plate as shown in Fig. 4.3(a). Similar failure can be seen in carbon surfaced functionally graded and sandwich hybrid plates as shown in Fig. 4.3(c) and 4.3(e), respectively. In case of plain GFRP plate and glass surfaced FH and SH plates buckling occurred near the loading edge but the failure of plates propagated from the corner of the plate as shown in Fig. 4.3(b), 4.3(d), and 4.3(f). This type of damage evolution was observed in the plates investigated numerically. The data obtained were recorded and the load vs. out-of-plane displacement graphs are plotted for all the plates tested. Load vs. out-of-displacement plots of postbuckling response of experimentally investigated composite plates have been depicted in Fig. 4.5.

The plain CFRP plate which is non-hybrid has the highest buckling load with fiber aligned in (0/90) directions, whereas the lowest buckling load was observed in non-hybrid GFRP plate. This is due to high stiffness of CFRP plates. As mentioned earlier, two different layup sequences are modeled and tested in this study. One is sandwich hybrid and the other is functionally graded hybrid. The buckling load values of these hybrid plates were investigated which lies in-between buckling load values of CFRP and GFRP. Carbon fiber surfaced (glass fiber in the core) functionally graded hybrid plate has higher buckling load with respect to plates with glass fiber in

the surface (carbon fiber in the core). The buckling loads (BL) of all the plates without cutouts are presented in Table 4.4 and in Fig. 4.5.

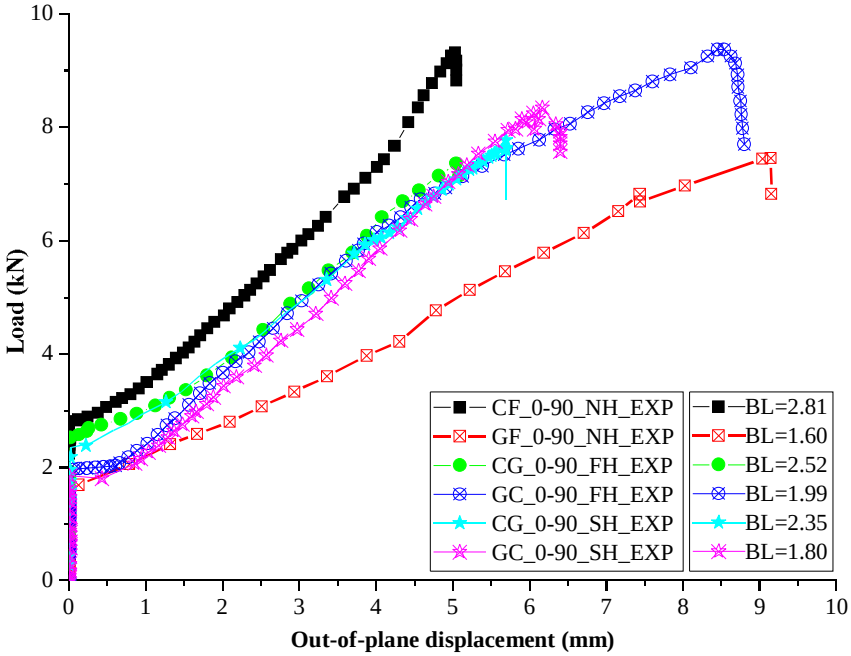

Fig. 4.5. Experimental postbuckling response of plain and hybrid laminates of fiber aligned in (0/90) direction under uniaxial compression without cutouts

The maximum out of plane displacement occurred just above the center of plate towards the loading direction as shown in Fig. 4.3(g). Similar response was observed in numerical analysis performed using ABAQUS. Comparison plots of experimental and numerical load vs. out-of-plane displacement of non-hybrid and hybrid composite plates are shown in Fig. 4.6. 'EXP' in the plate ID represents experimental and 'ABQ' represents numerical results. Experimental buckling loads are in good agreement with the numerically calculated buckling loads.

4.3.2. Numerical study

4.3.2.1. Buckling load

The plates are simulated numerically using finite element based software ABAQUS and the buckling mode shapes of functionally graded hybrid plate obtained are shown in Fig. 4.7. The mode shapes I, II and III are shown in Figs. 4.7(a), 4.7(b), and 4.7(c), respectively. Mode-I buckling shape has one half longitudinal wave towards the loading edge, which is similar to the buckling mode shape obtained in the experimental studies as depicted in Fig. 4.3. Mode-II buckling

shape also has one half longitudinal wave, but it is away from the loading edge. In mode-III buckling, length of the plate is divided into three longitudinal waves as shown in Fig. 4.7(c). Since mode-I buckling shape is like the experimental buckling shape, the eigen value obtained in this mode is considered as buckling mode. Initially, buckling loads of all composite plates are obtained using linear eigen value analysis and are shown in Fig. 4.8. The buckling loads obtained from experiment are in good agreement with the numerical buckling loads as shown in Fig. 4.5.

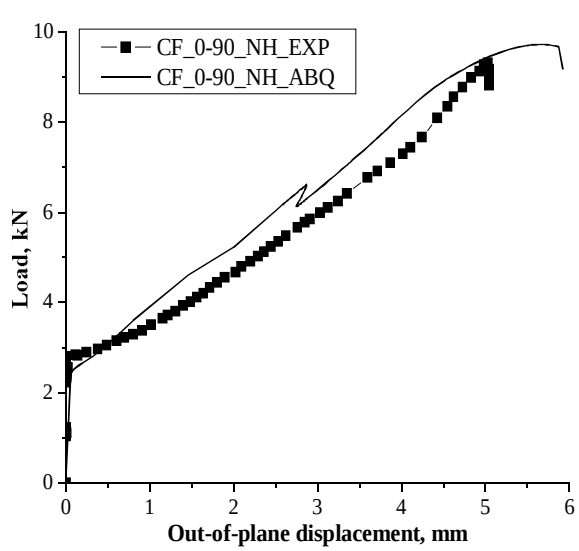

(a)

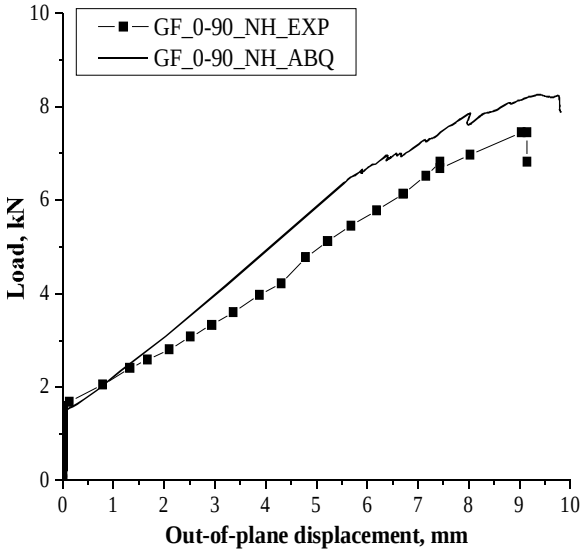

(b)

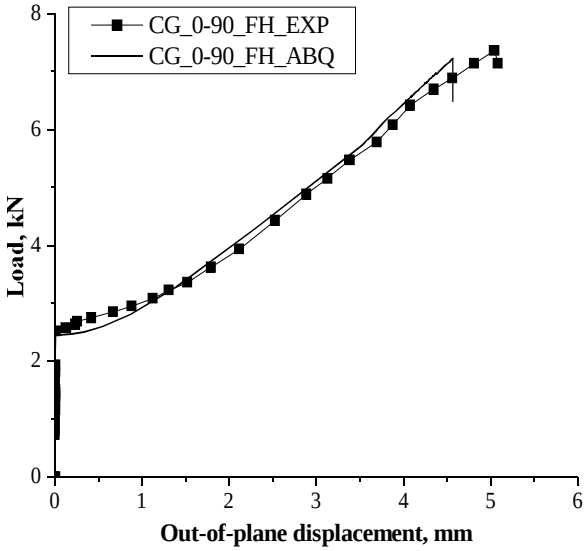

(c)

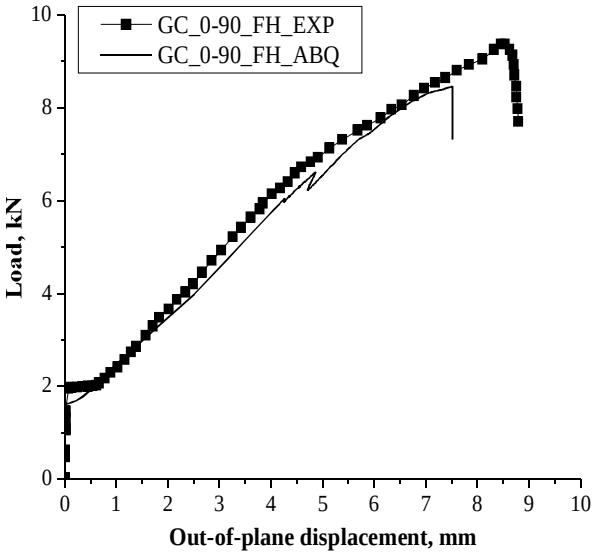

(d)

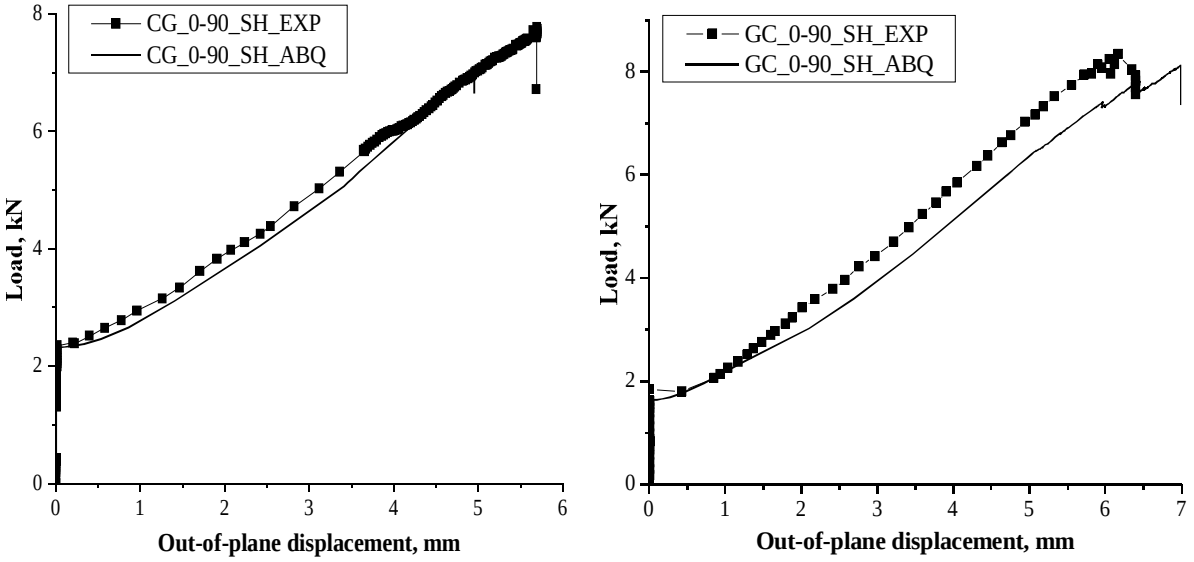

(e) (f)

Fig. 4.6. Comparison graphs between experimental (EXP) and numerical (ABQ) postbuckling strengths of laminates: (a) CF_$(0/90)_{4s}$_NH (b) GF_$(0/90)_{4s}$_NH (c) CG_$(0/90)_{4s}$_FH (d) GC_$(0/90)_{4s}$_FH (e) CG_$(0/90)_{4s}$_SH (f) GC_$(0/90)_{4s}$_SH

Later, postbuckling analysis of these plates is investigated using non-linear static-riks analysis from which load vs. out-of-plane displacement plots are obtained. Fig. 4.9 depicts load vs out-of-displacemnt plots of composite plates without cutouts obtained from numerical simulation. Fig. 4.9(a) shows the plots of the plates with fiber aligned in (0/90) direction. Load-displacement plots of plates with fiber aligned in (-45/+45) and (-45/+45/0/90) are shown in Figs. 4.9(b) and 4.9(c), respectively.

Experimental postbuckling analysis is conducted only on plates with fiber aligned in $(0/90)_{4s}$ direction without cutouts and these results are validated with numerically obtained results. Figure 4.6 shows the comparison between obtained loads vs. out-of-plane displacements responses. In Fig. 4.6(a), postbuckling response of plate with fiber aligned in $(0/90)_{4s}$ direction are compared in which experimental buckling load is 2.5% higher than numerical buckling load. Thus, experimental and numerical results are close. In all the plates tested, experimental buckling load values are higher than numerical values with a minor difference and the percentage increase is given in Table 4.4.

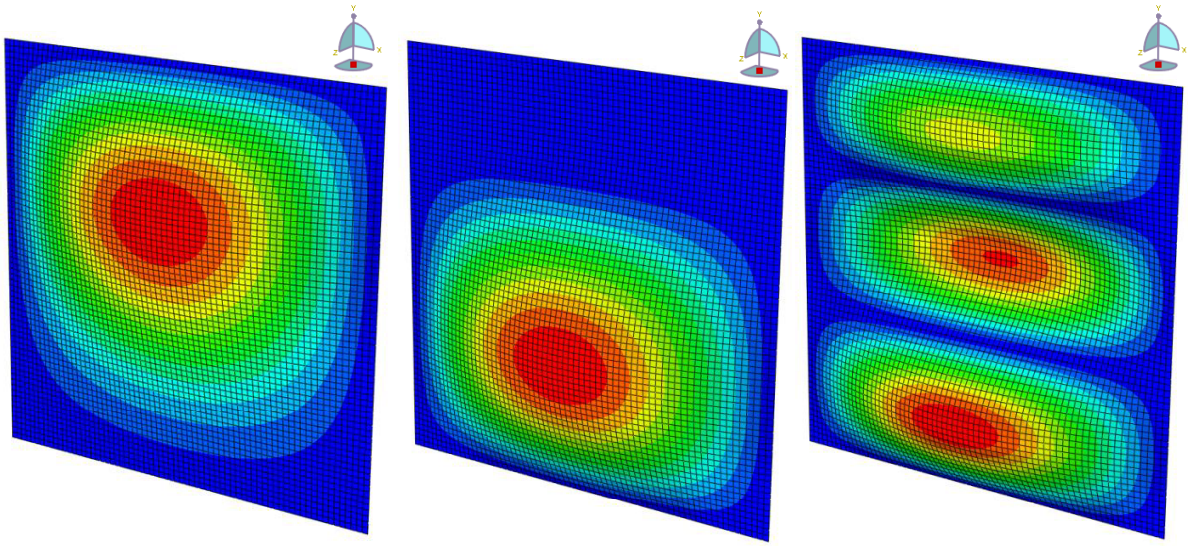

(a) (b) (c)

Fig. 4.7. Buckling mode shapes of the functionally graded hybrid plate analyzed using numerical simulation under uniaxial compression buckling load: (a) Mode-I buckled shape (b) Mode-II buckled shape (c) Mode-III buckled shape

Amongst the plates analyzed experimentally and numerically, carbon fiber reinforced polymer (CFRP) plates have highest buckling and postbuckling strengths whereas glass fiber reinforced polymer plates have lowest buckling and postbuckling strengths. In case of plates with fiber aligned in $(0/90)_{4s}$ direction, CFRP plate is observed to resist highest buckling load than other plates.

Table 4.4. Comparison of buckling loads determined using experimental and numerical study without cutouts

Specimen ID	Experimental buckling load, kN	Numerical buckling load, kN	Difference, %
CF_0-90_NH	2.81	2.74	2.5
GF_0-90_NH	1.60	1.59	0.6
CG_0-90_FH	2.52	2.45	2.8
GC_0-90_FH	1.99	1.92	3.5
CG_0-90_SH	2.35	2.32	1.2
GC_0-90_SH	1.80	1.64	8.9

It is also observed that CFRP and carbon fiber surfaced plates have low out-of-plane displacement compared to GFRP plates and other glass fiber surfaced plates. Since, the experimental and numerical results of the plates with fiber aligned in $(0/90)_{4s}$ direction agree well with each other, a parametric study was conducted considering two other different types of plates in which fiber is

aligned in $(-45/+45)_{4s}$ and $(-45/+45/0/90)_{2s}$ directions. In Fig. 4.8, buckling loads of non-hybrid and hybrid plates are presented. From this, it is worth noting that, plates having stacking sequence of $(-45/+45/0/90)_{2s}$ are having highest buckling loads. In CFRP plates with stacking sequence $(-45/+45/0/90)_{2s}$, the buckling load is almost 50% higher than plates with $(0/90)_{4s}$ stacking sequence and 11% higher than plates with $(-45/+45)_{4s}$ stacking sequence while in case of GFRP plates, it is 32% and 2.5% higher than plates with $(0/90)_{4s}$ and $(-45/+45)_{4s}$ stacking sequence, respectively. It is observed that, there is a considerable increase in buckling loads in $(-45/+45/0/90)_{2s}$ fiber-oriented plates of functionally graded hybrid layup sequence compared to $(0/90)_{4s}$ and $(-45/+45)_{4s}$ fiber-oriented plates. But, in case of sandwich hybrid plates with fiber aligned in $(-45/+45)_{4s}$ and $(-45/+45/0/90)_{2s}$ direction, buckling load values are approximately same. Also, functionally graded hybrid plates have higher buckling loads compared to sandwich hybrid plates. Therefore, functionally graded hybrid plates surfaced with carbon fiber (glass fibers in the core) with $(-45/+45/0/90)_{2s}$ stacking sequence are more effective for structural applications as far as buckling load is considered as failure load.

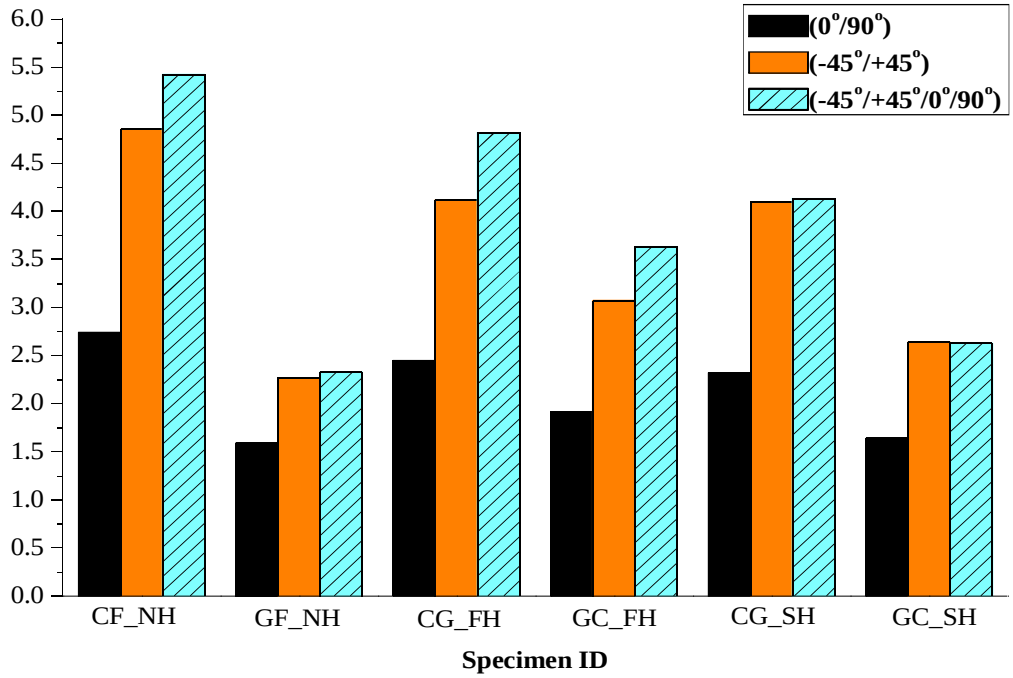

Fig. 4.8. Numerical buckling loads of non hybrid, functionally graded hybrid and sandwich hybrid plates in which fiber is aligned in (0/90), (-45/+45) and (-45/+45/0/90) directions without cutouts

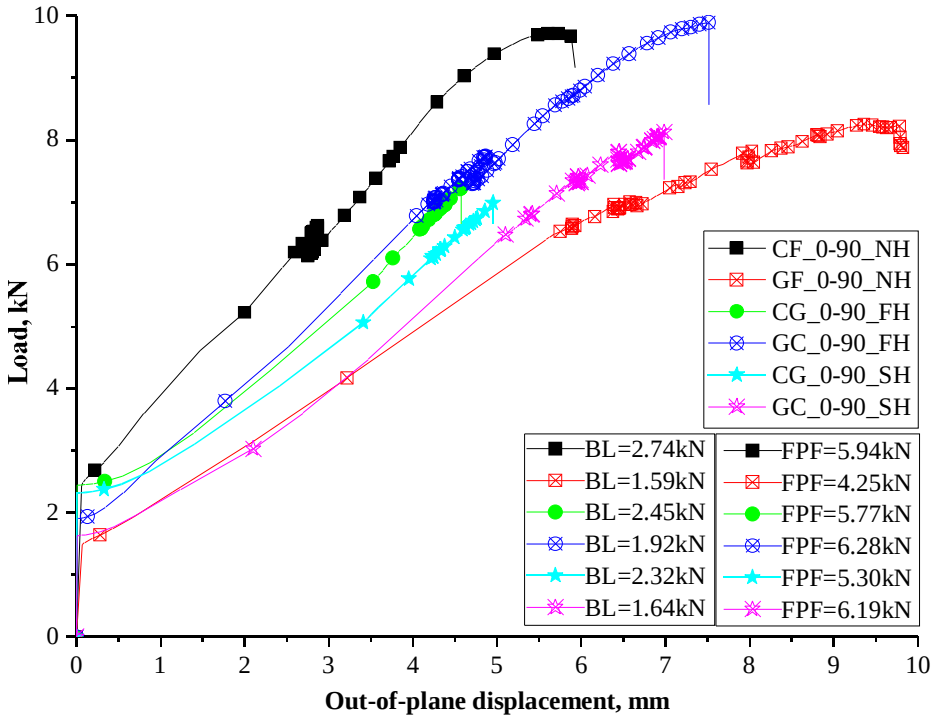
Load, kN
Out-of-plane displacement, mm
CF_0-90_NH
GF_0-90_NH
CG_0-90_FH
GC_0-90_FH
CG_0-90_SH
GC_0-90_SH
BL=2.74kN
BL=1.59kN
BL=2.45kN
BL=1.92kN
BL=2.32kN
BL=1.64kN
FPF=5.94kN
FPF=4.25kN
FPF=5.77kN
FPF=6.28kN
FPF=5.30kN
FPF=6.19kN

(a)

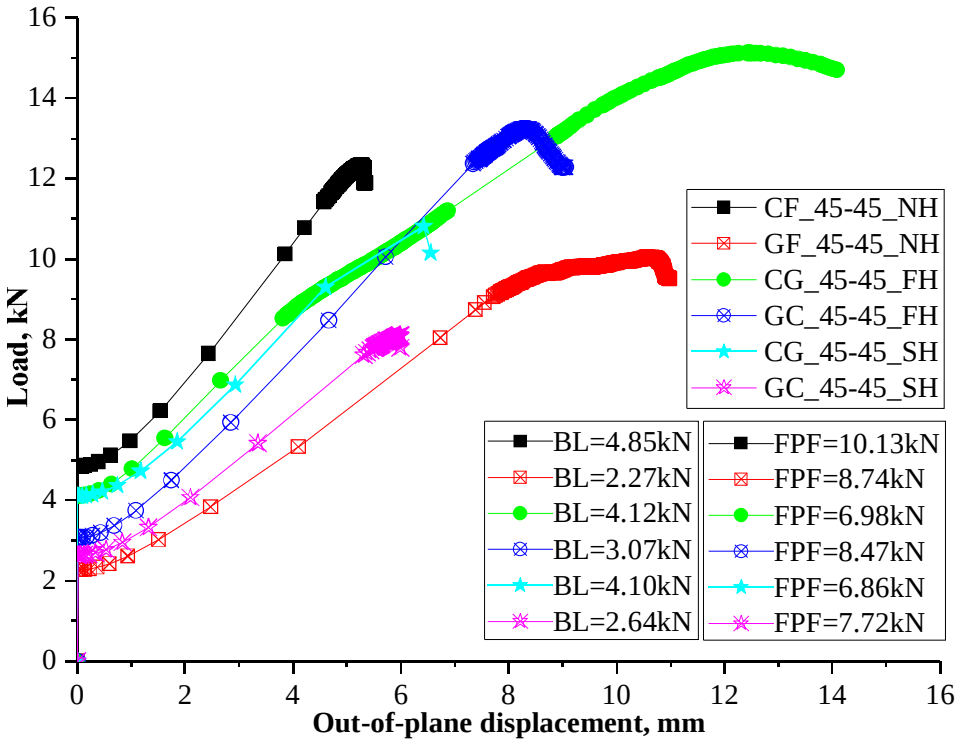
Load, kN
Out-of-plane displacement, mm
CF_45-45_NH
GF_45-45_NH
CG_45-45_FH
GC_45-45_FH
CG_45-45_SH
GC_45-45_SH
BL=4.85kN
BL=2.27kN
BL=4.12kN
BL=3.07kN
BL=4.10kN
BL=2.64kN
FPF=10.13kN
FPF=8.74kN
FPF=6.98kN
FPF=8.47kN
FPF=6.86kN
FPF=7.72kN

(b)

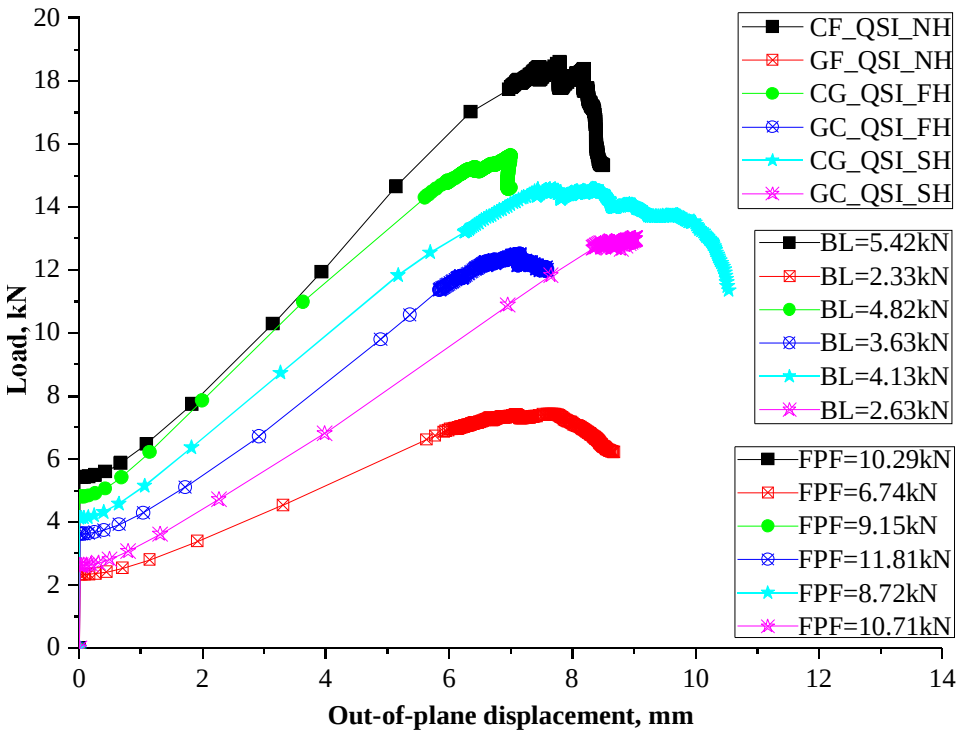

(c)

Fig. 4.9. Numerical postbuckling response of non-hybrid and hybrid plates without cutouts aligned in various fiber directions: (a) $(0/90)_{4s}$ (b) $(-45/+45)_{4s}$ (c) $(-45/+45/0/90)_{2s}$

4.3.2.2. First ply failure load

Tsai-Hill failure criterion has been incorporated to determine the first ply failure (FPF) or first ply failure of the composite plates. The FPF occurs when the failure index in a plate is greater than or equal to 1. During non-linear static-riks analysis, the plate at an increment reaches value 1 or greater than it. The load corresponding to that increment is the first ply failure load. The FPF loads of all the composite plates are given in Table 4.5. The FPF loads of CFRP and carbon fiber surfaced (glass fiber in the core) plates is approximately twice the buckling load. It is three times the buckling load in case of GFRP and glass fiber surfaced (carbon fiber in the core) composite plates. It is evident that functionally graded hybrid composite plate with glass fiber as surface has the highest first ply failure load among the hybrid plates with $(-45/+45/0/90)_{2s}$ stacking sequence. It is also observed that the same plate has highest first ply failure load for all the stacking sequences. Even in carbon surfaced hybrid plates, functionally graded hybrid plates are dominant as far as first ply failure loads are concerned.

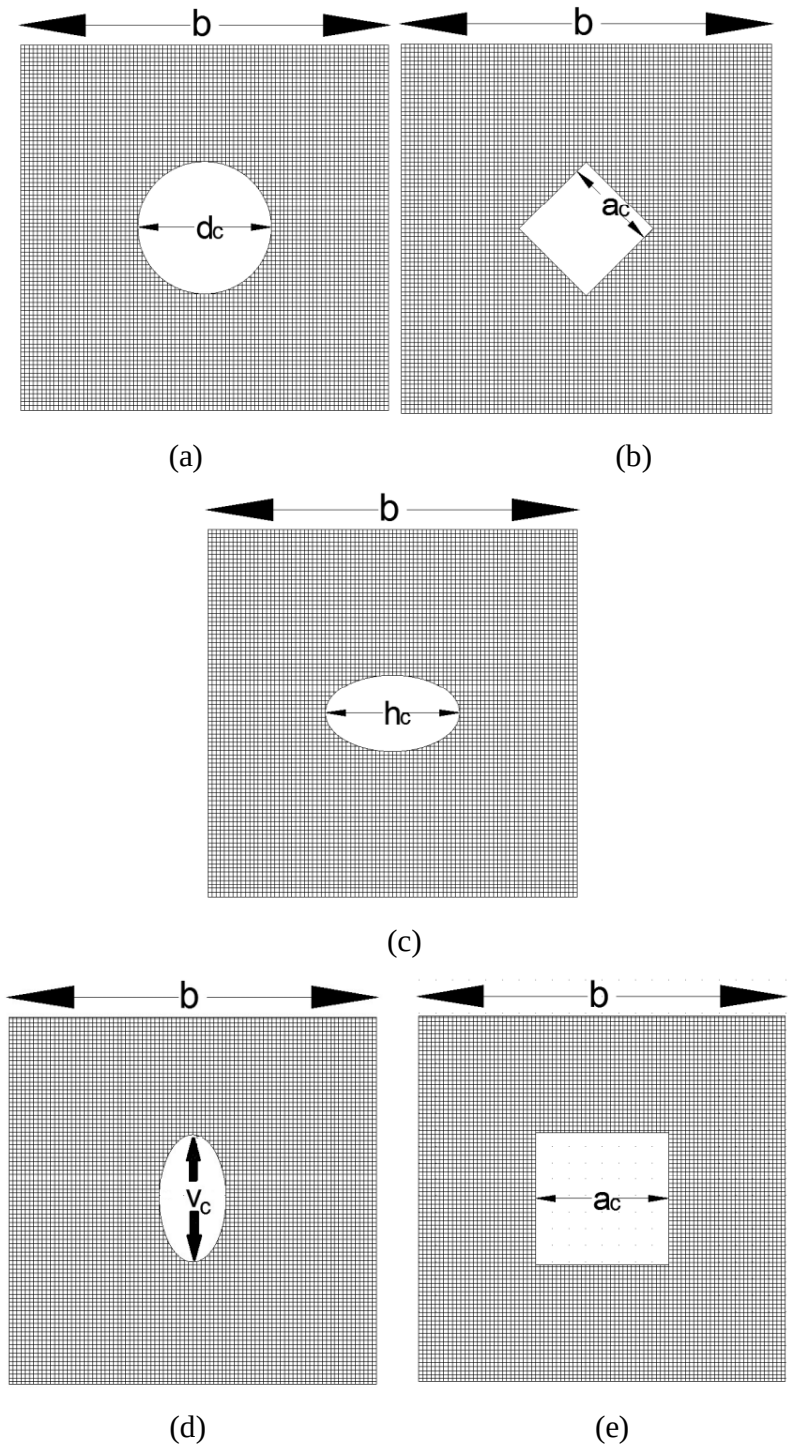

Fig. 4.10. Cutout shapes of the composite plates used in this study: (a) Circular cutout (b) Diamond cutout (c) Ellipse-horizontal cutout (d) Ellipse-vertical cutout (e) Square cutout

4.3.3. Effect of cutouts

Further, effect of cutouts on buckling and postbuckling responses has been examined using numerical analysis in which different shaped and sized cutouts were considered as shown in Table 4.6 and Fig. 4.10.

Table 4.5. Buckling and first ply failure loads of non-hybrid and hybrid laminates determined using ABAQUS without cutouts

Specimen ID	Buckling load (BL), kN	First ply failure load, kN	FPF/BL ratio
CF_0-90_NH	2.74	5.94	2.17
GF_0-90_NH	1.59	4.25	2.67
CG_0-90_FH	2.45	5.77	2.36
GC_0-90_FH	1.92	6.28	3.27
CG_0-90_SH	2.32	5.30	2.28
GC_0-90_SH	1.64	6.19	3.77
CF_45-45_NH	4.85	10.13	2.09
GF_45-45_NH	2.27	8.74	3.85
CG_45-45_FH	4.12	6.98	1.69
GC_45-45_FH	3.07	8.47	2.76
CG_45-45_SH	4.10	6.86	1.67
GC_45-45_SH	2.64	7.72	2.92
CF_QSI_NH	5.42	10.29	1.90
GF_QSI_NH	2.33	6.74	2.89
CG_QSI_FH	4.82	9.15	1.90
GC_QSI_FH	3.63	11.81	3.25
CG_QSI_SH	4.13	8.72	2.11
GC_QSI_SH	2.63	10.71	4.07

Table 4.3 gives the nomenclature of functionally graded composite plates with cutouts. The buckling loads are determined using linear Eigen value analysis and the values are presented in Table 4.7. A comparison bar chart is made as shown in Fig. 4.11 from which it is noted that plates with stacking sequence $(-45/+45/0/90)_{2s}$ have highest buckling load. It is also evident that plates with smaller size cutout perform better in terms of buckling load. Among the five cutout shapes considered in this study, diamond shaped cutout and ellipse aligned horizontal shaped cutout have higher buckling loads than those of other cutout shapes. Even though the ellipse aligned horizontal shaped cutout has the highest buckling load compared to diamond shaped cutout, the difference is negligible. The load vs. out-of-plane displacement plots are made for all the composite plates with smaller size cutouts considering all the three stacking sequences. The first ply failure load and the ultimate failure load can be observed clearly from this plot. The comparison is made only between

plates with smaller cutouts made of carbon fiber surfaced functionally graded hybrid composite plates since the main objective of this study is to verify the buckling and postbuckling response of hybrid composite plates.

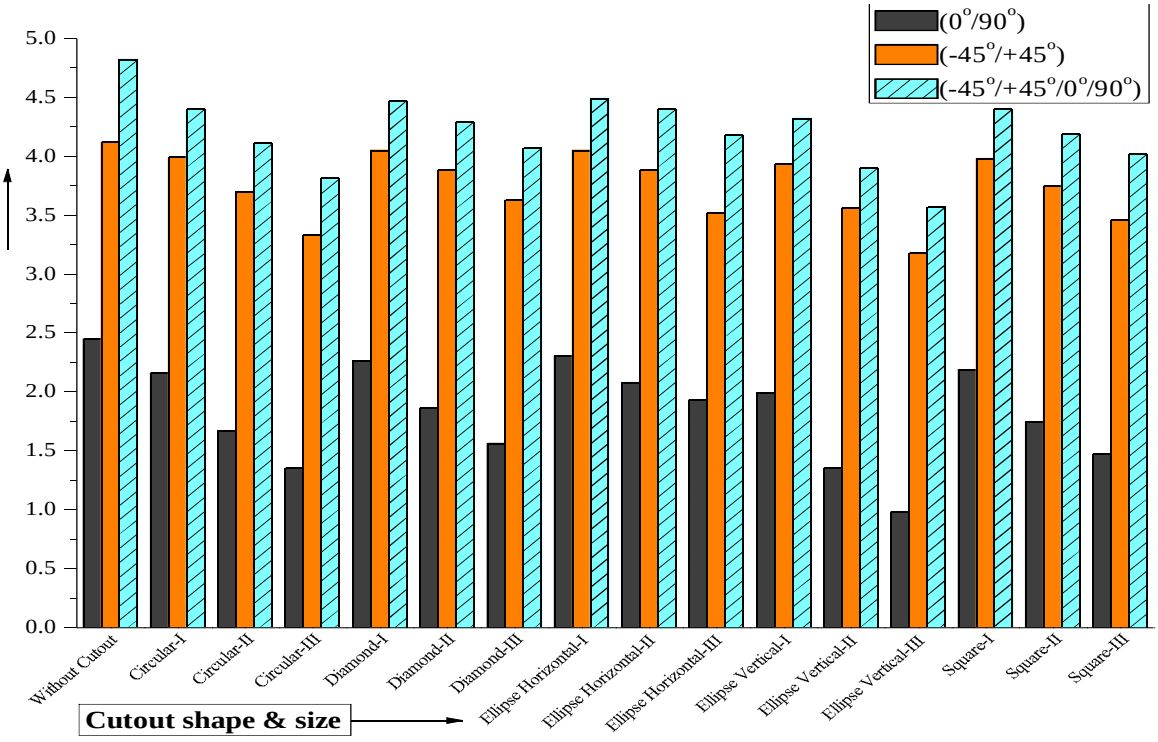

Fig. 4.11. Buckling loads of functionally graded hybrid composite plates with and without cutouts stacked with fiber aligned in $(0/90)_{4s}$, $(-45/+45)_{4s}$, and $(-45/+45/0/90)_{2s}$ directions

Table 4.6. Cutout specifications

Shape of cutout* / Size of cutout*	1 (Small)	2 (Medium)	3 (Big)
Circle (d_c/b)	0.158	0.316	0.474
Diamond (a_c/b)	0.140	0.280	0.420
Ellipse horizontal (h_c/b)	0.224	0.447	0.670
Ellipse vertical (v_c/b)	0.112	0.223	0.335
Square (a_c/b)	0.140	0.280	0.420

*b=dimensions of square plate in x and y directions; d_c=diameter of circular cutout; a_c=side dimension of square and diamond cutout; h_c=length of major axis of ellipse cutout; v_c=length of minor axis of ellipse cutout

Crack propagation in the functionally graded hybrid composite plates with and without cutouts is shown in Fig. 4.12. Plates with small sized cutouts with various shaped cutouts are shown in Figs.

4.12(b), 4.12 (c), 4.12(d), 4.12(e), and 4.12(f). The fiber direction in all the plates is $(0/90)_{4s}$. The corresponding first ply failure loads have been depicted in the figure caption as well as in Fig. 4.13(a). Cracks started near the loading edge in all the plates simulated numerically. Similar trend was observed in experimentally investigated composite plates. Since the crack propagation is similar in medium and large sized cutouts, only figures with smaller sized cutouts are shown.

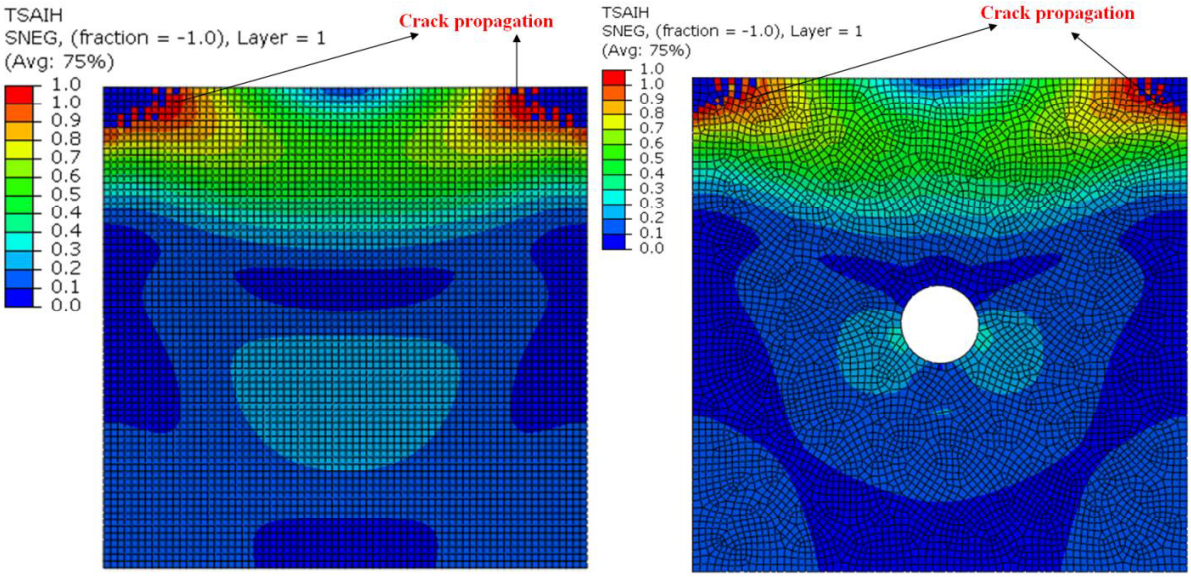

(a) (b)

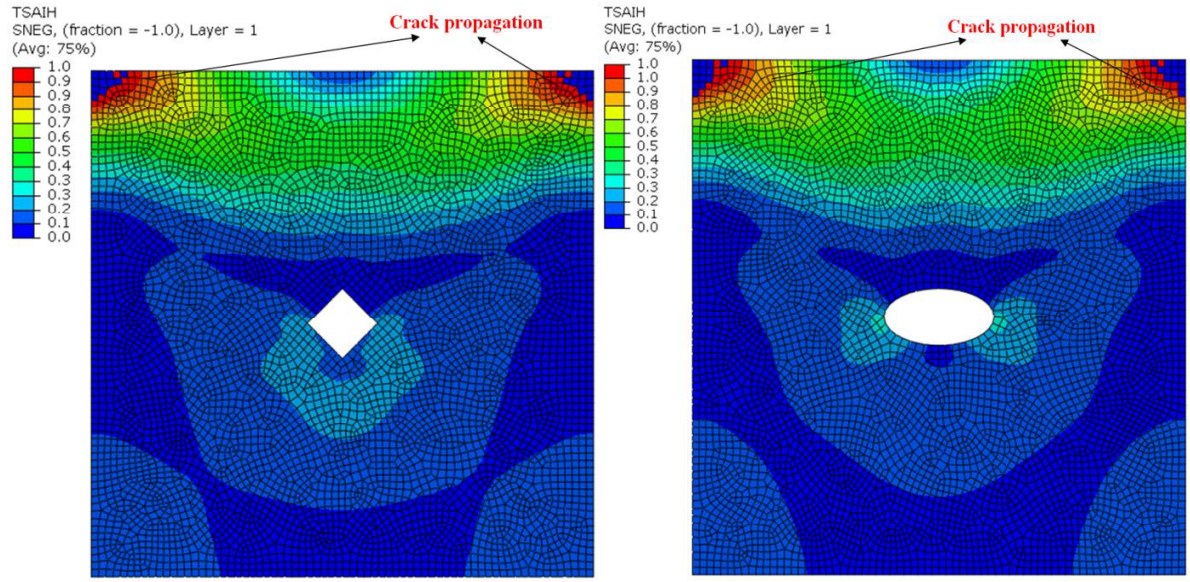

(c) (d)

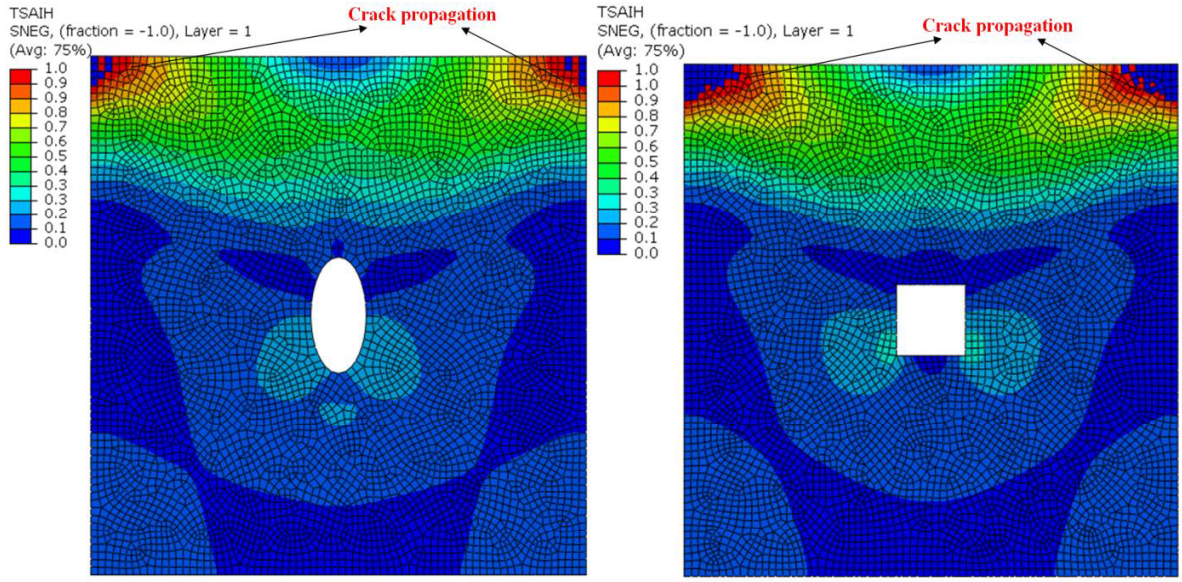

(e) (f)

Fig. 4.12. Initial crack propagation observed in functionally graded composite plates with and without cutouts with fiber aligned in (0/90) direction. The corresponding loads (in kN) are given in paranthesis: (a) FH_CG_NC (5.77) (b) FH_CG_C1 (3.95) (c) FH_CG_D1 (4.42) (d) FH_CG_EH1 (5.63) (e) FH_CG_EV1 (4.20) (f) FH_CG_S1 (3.99)

4.3.3.1. $(0/90)_{4s}$ stacking sequence

The load versus maximum out-of-plane displacement curves of functionally graded hybrid plates with different shaped cutouts with small, medium, and big size and fiber aligned in $(0/90)_{4s}$ direction are detailed below.

4.3.3.1.1. Small size cutouts

In Fig. 4.13(a), the load vs. out-of-plane displacement plots of carbon fiber surfaced functionally graded hybrid composite plates having $(0/90)_{4s}$ stacking sequence can be seen for smaller size cutout. The maximum buckling load can be observed for carbon surfaced functionally graded hybrid plate with elliptical cutout aligned horizontally (CG_FH_EH1_$(0/90)_{4s}$) which is 6%, 1.73%, 13.4%, and 4.78% higher with respect to the plates with circular, diamond, ellipse-vertical, and square shaped cutout, respectively. Further, maximum first ply failure load is also observed in CG_FH_EH1_$(0/90)_{4s}$ plate as shown in Fig. 4.13(a). During the postbuckling deformation, it is worth noting that first ply failure load of the plate is twice the buckling load and ultimate failure load is about four times the buckling load which is significant.

Table 4.7. Buckling and first ply failure loads of functionally graded hybrid plates with and without cutouts

Specimen ID	Cutout size	Buckling and first ply failure loads (kN) corresponding to layup sequence of the composite plate		
		$(0/90)_{4s}$	$(-45/+45)_{4s}$	$(-45/+45/0/90)_{2s}$
FH_CG_NC	-	2.45(5.77)*	4.12(6.98)*	4.82(9.15)*
FH_CG_C	1 (small)	2.16(3.95)	3.99(6.78)	4.40(10.03)
	2 (medium)	1.67(4.11)	3.70(6.42)	4.11(9.91)
	3 (big)	1.35(3.84)	3.33(5.91)	3.81(10.60)
FH_CG_D	1 (small)	2.26(4.42)	4.05(6.74)	4.47(10.73)
	2 (medium)	1.86(5.54)	3.88(6.63)	4.29(9.99)
	3 (big)	1.56(5.95)	3.63(8.33)	4.07(9.72)
FH_CG_EH	1 (small)	2.30(5.63)	4.04(6.93)	4.49(11.51)
	2 (medium)	2.08(4.60)	3.88(7.98)	4.40(11.55)
	3 (big)	1.93(4.70)	3.52(7.11)	4.18(11.31)
FH_CG_EV	1 (small)	1.99(4.20)	3.93(6.58)	4.32(10.40)
	2 (medium)	1.35(5.36)	3.56(7.46)	3.90(7.15)
	3 (big)	0.98(3.76)	3.18(8.02)	3.57(9.03)
FH_CG_S	1 (small)	2.19(3.99)	3.98(6.63)	4.40(10.68)
	2 (medium)	1.75(4.91)	3.75(10.32)	4.19(11.52)
	3 (big)	1.47(4.95)	3.46(6.35)	4.02(9.77)

*Quantities in parenthesis are first ply failure loads

4.3.3.1.2. Medium size cutouts

The buckling and first ply failure load of carbon surfaced functionally graded composite plates with medium sized cutouts are depicted in Fig. 4.13(b). CG_FH_EH2_$(0/90)_{4s}$ specimen has the highest buckling load amongst all medium sized cutout specimens aligned in $(0/90)_{4s}$ stacking sequence as shown in Fig. 4.13(b) while the highest first ply failure load can be observed in case of plate with diamond shaped cutout. Peak buckling load of CG_FH_EH2_$(0/90)_{4s}$ specimen is 19.71%, 10.57%, 35.57%, and 15.86% higher with respect to the plates with circular, diamond, ellipse-vertical, and square shaped cutouts respectively. It is also observed that first ply failure load is approximately 2.9 times the buckling load on an average of all the plates.

4.3.3.1.3. Big size cutouts

The load vs. displacement plots of carbon surfaced functionally graded composite plates with big sized cutouts are shown in Fig. 4.13(c). Similar trend such as medium sized cutout plates can be observed in big sized cutout plates in case of both buckling load and the first ply failure load. From

Fig. 4.13(c), it is observed that the buckling load of the composite plate with elliptical cutout aligned horizontally is almost twice the buckling load of plate with elliptical cutout aligned vertically. This is due to the lesser distance between the loading edge and the cutout edge located towards the loading point. The buckling loads are 30.56%, 19.68%, 49.74%, and 24.35% lower than peak buckling load specimen CG_FH_EH3_$(0/90)_{4s}$ with respect to circular, diamond, ellipse-vertical, and square shaped cutout plates respectively. In this case, first ply failure load is approximately 3.28 times the buckling load on an average of all the plates.

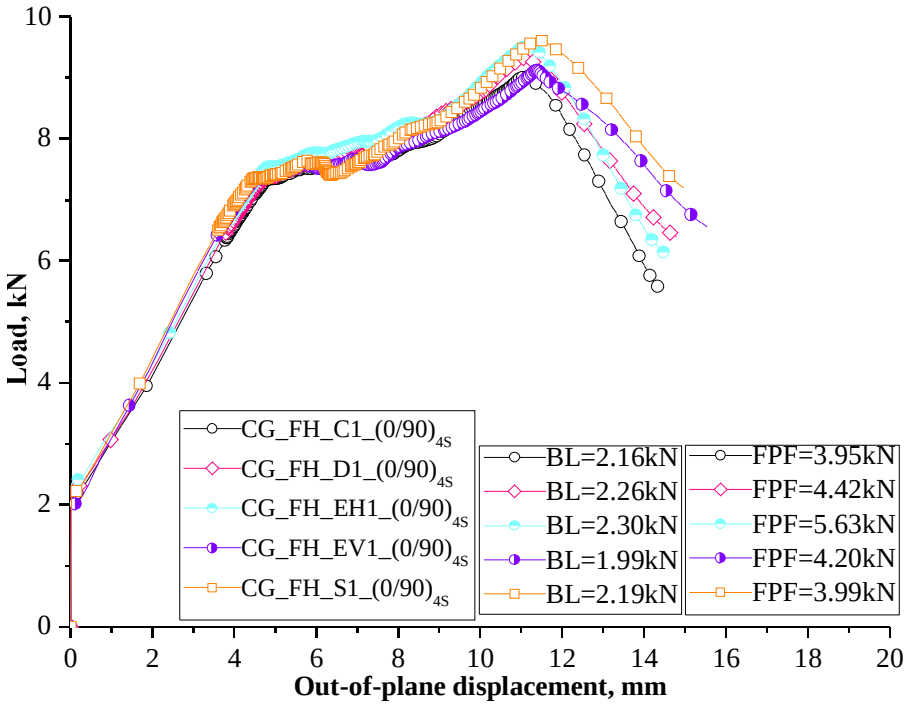

(a)

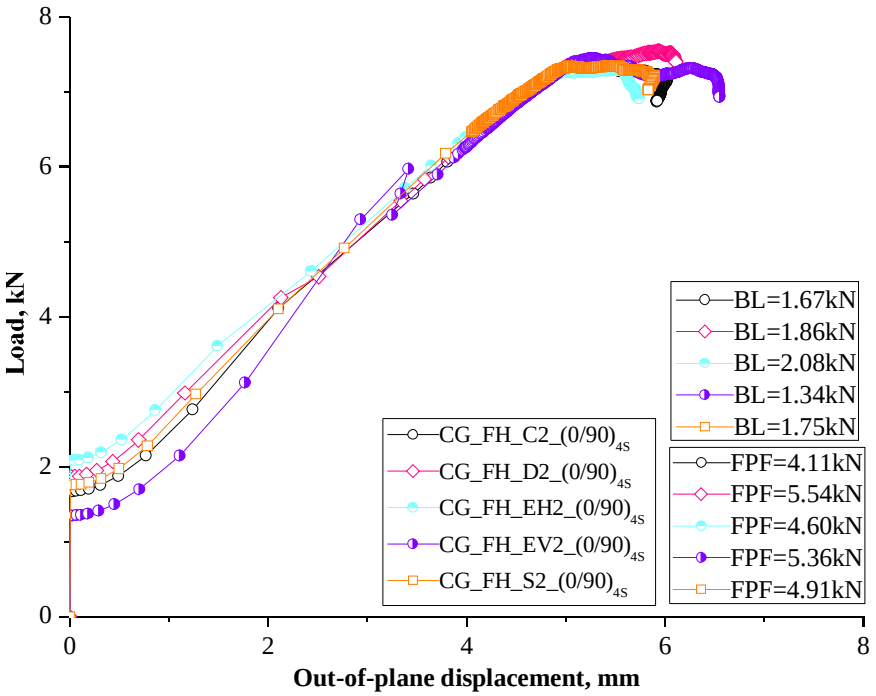

(b)

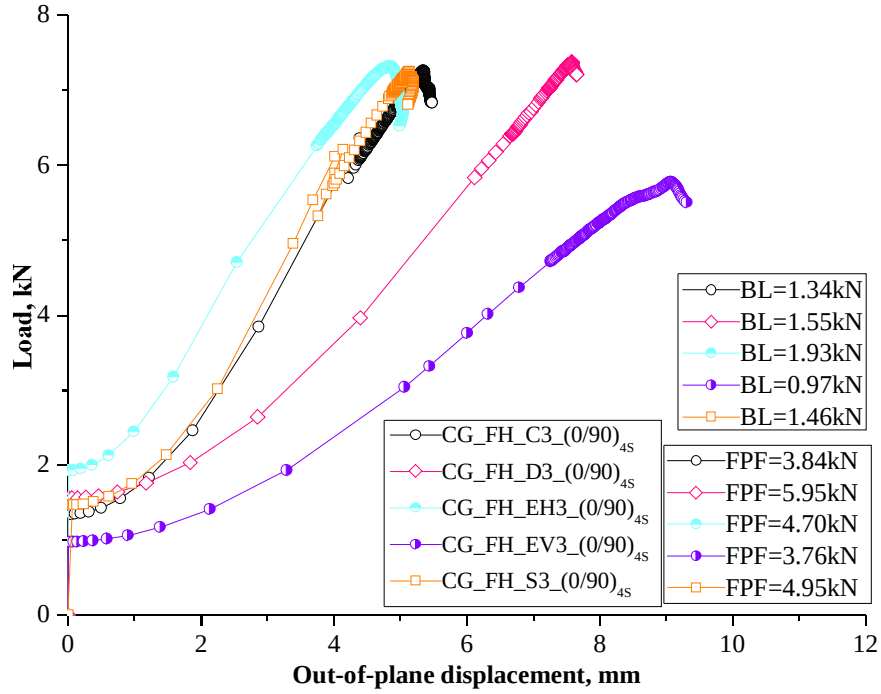

(c)

Fig. 4.13. Load vs. displacement curves of functionally graded hybrid plates with various shaped and sized cutouts stacked in $(0/90)_{4s}$ fiber direction: (a) Small size cutout (b) Medium size cutout (c) Big size cutout

4.3.3.2. (-45/+45)4s stacking sequence

The load versus maximum out-of-plane displacement curves of functionally graded hybrid plates with different shaped having small, medium, and big sized cutout plates with fiber aligned in $(-45/+45)_{4s}$ direction are described below. Crack propagation in the plates with fiber aligned in $(-45/+45)_{4s}$ direction is shown in Fig. 4.14 where Fig. 4.14(a) depicts the plate without cutout. Figs. 4.14(b), 4.14(c), 4.14(d), 4.14(e), and 4.14(f) show the plates with different shaped cutouts such as circle, diamond, ellipse-horizontal, ellipse-vertical, and square cutouts, respectively.

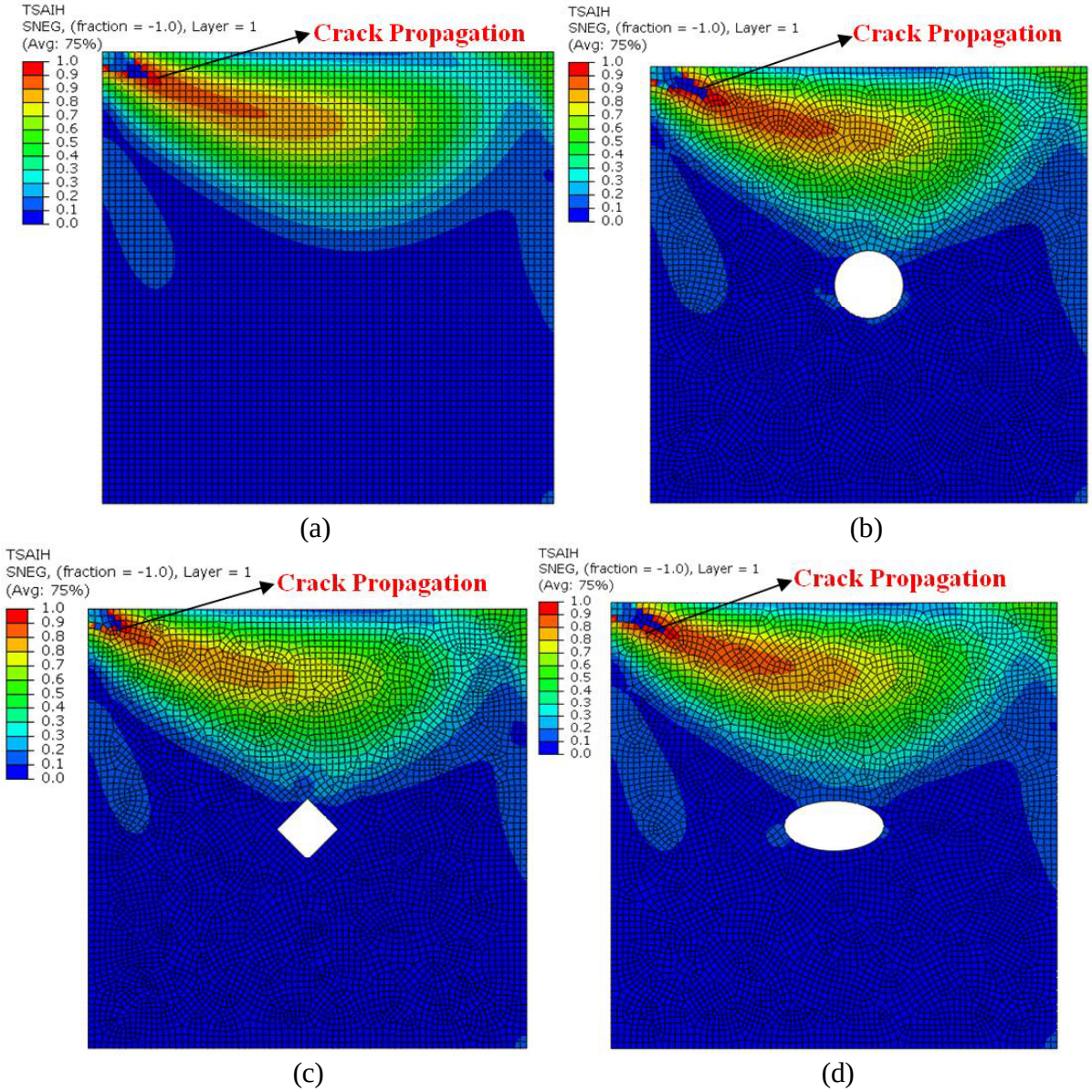

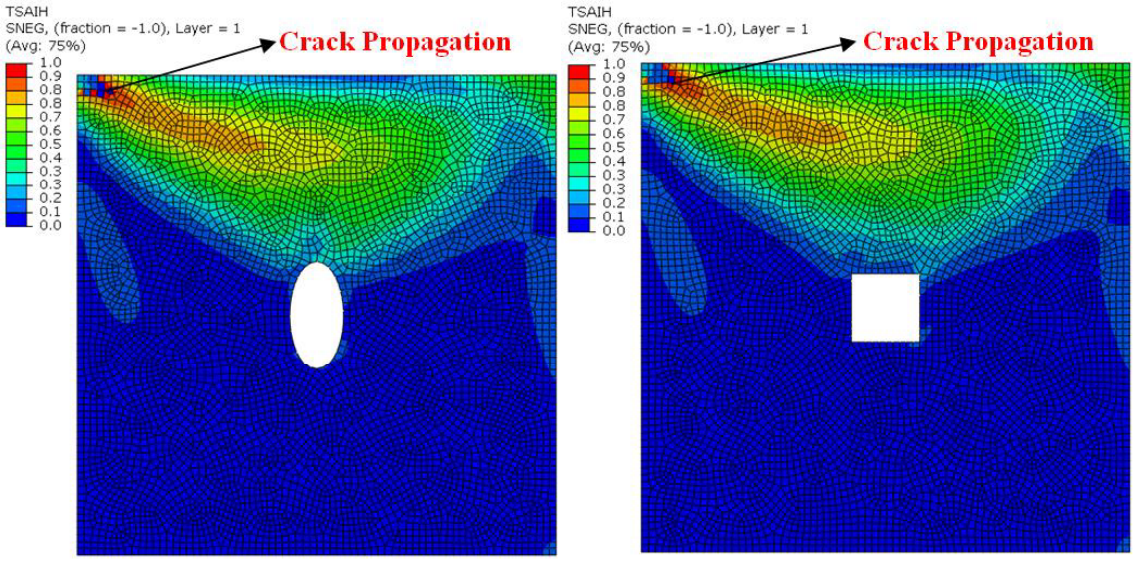

(e) (f)

Fig. 4.14. Initial crack propagation observed in functionally graded composite plates with and without cutouts with fiber aligned in (-45/+45) direction. The corresponding first ply failure loads (in kN) are given in paranthesis: (a) FH_CG_NC (6.98) (b) FH_CG_C1 (6.78) (c) FH_CG_D1 (6.74) (d) FH_CG_EH1 (6.93) (e) FH_CG_EV1 (6.58) (f) FH_CG_S1 (6.63)

Unlike crack propagation in plates with stacking sequence $(0/90)_{4s}$, crack started from only one edge. Therefore, composite plates in which fiber is aligned in $(-45/+45)_{4s}$ direction have higher load carrying capacity than plates with fiber aligned in $(0/90)_{4s}$ direction. The corresponding first ply failure loads are shown in Fig. 4.15(a) and Table 4.7.

4.3.3.2.1. Small size cutouts

In Fig. 4.15(a), the load vs. out-of-plane displacement plots of carbon fiber surfaced functionally graded hybrid composite plates having $(-45/+45)_{4s}$ stacking sequence are shown. The maximum buckling load can be observed for CG_FH_D1_$(-45/+45)_{4s}$ plate which has respectively 1.48%, 0.24%, 2.96%, and 1.72% higher buckling loads than those of the circular, ellipse-horizontal, ellipse-vertical, and square shaped cutouts. But the maximum first ply failure load is not same like the buckling load and this can be observed in CG_FH_EH1_$(-45/+45)_{4s}$ plate as shown in Fig. 4.15(a). During postbuckling of these plates, first ply failure load is 1.5 times the buckling load whereas ultimate failure load of these plates is about 2.75 times the buckling load.

4.3.3.2.2. Medium size cutouts

The buckling and first ply failure loads are depicted in Fig. 4.15(b). CG_FH_D2_$(-45/+45)_{4s}$ specimen has the highest buckling load amongst all medium sized cutout specimens aligned in plates with $(-45/+45)_{4s}$ stacking sequence as shown in Fig. 4.15(b). It is observed that the difference between buckling loads of composite plates with diamond shaped cutout and elliptical shaped cutout aligned horizontally is very less. Peak buckling load of CG_FH_D2_$(-45/+45)_{4s}$ specimen is 4.63%, 0.25%, 8.50%, and 3.35% higher with respect to the plates with circular, ellipse-horizontal, ellipse-vertical, and square shaped cutouts respectively. But, the first ply failure load is higher in case of CG_FH_S2_$(-45^o/+45^o)_{4s}$. It is also observed that the first ply failure load is almost twice the buckling load on an average for all the plates.

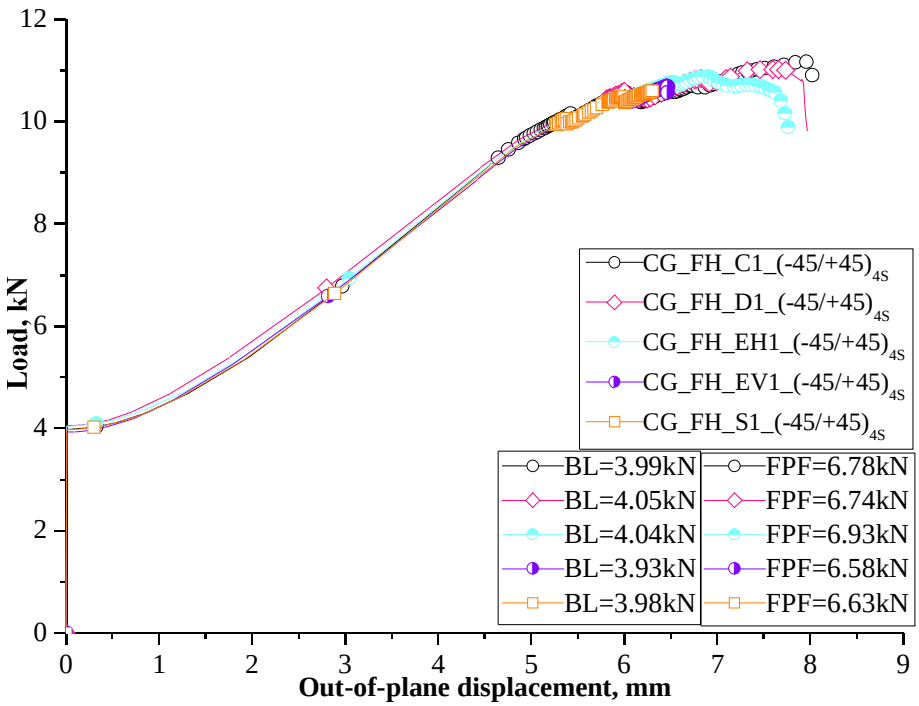

(a)

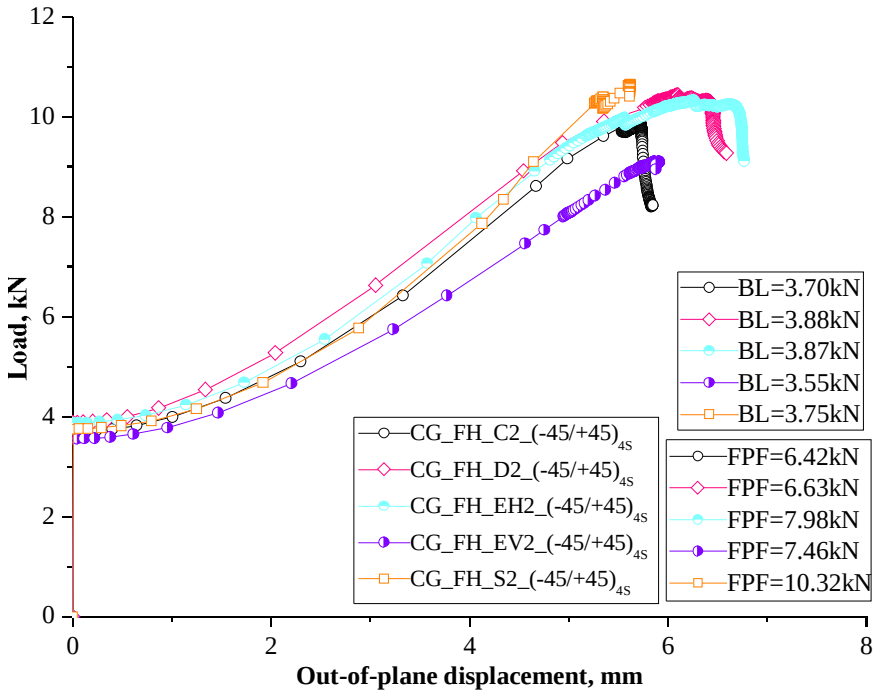

(b)

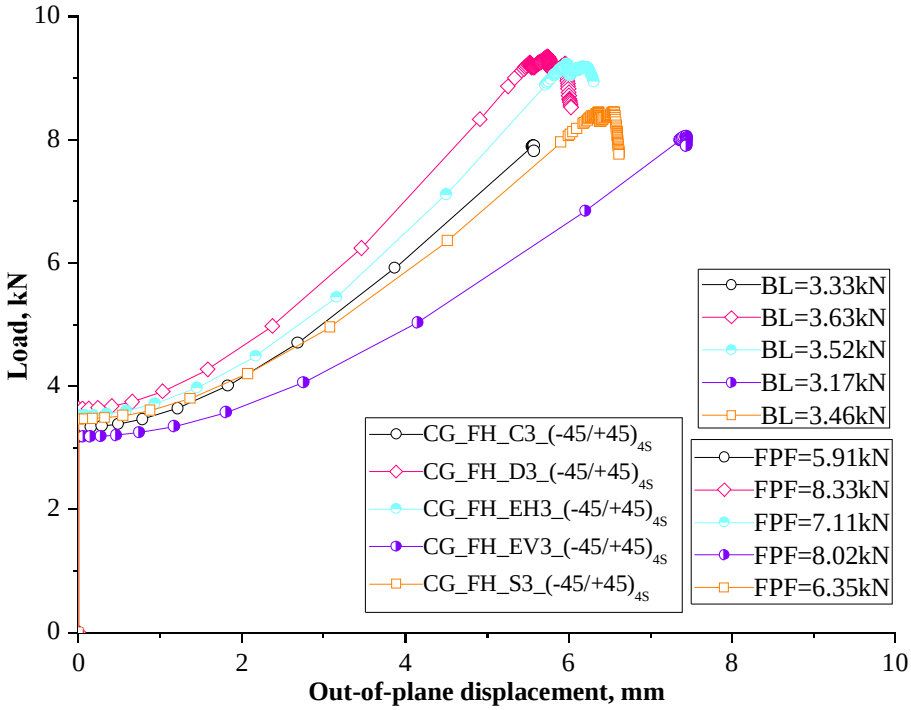

(c)

Fig. 4.15. Load vs. displacement curves of functionally graded hybrid plates with various shaped and sized cutouts stacked in $(-45/+45)_{4s}$ fiber direction: (a) Small size cutout (b) Medium size cutout (c) Big size cutout

4.3.3.2.3. Big size cutouts

The load vs. displacement plots of carbon surfaced functionally graded composite plates with big sized cutouts are shown in Fig. 4.15(c). The diamond shaped cutout functionally graded composite plate has higher buckling load than those with circular, ellipse-horizontal, ellipse-vertical, and square shaped cutouts. The buckling loads are 8.26%, 3.03%, 12.67%, and 4.68% lower for circular, ellipse horizontal, ellipse vertical, and square shaped cutouts, respectively. Also, CG_FH_D3_$(-45/+45)_{4s}$ specimen has the highest first ply failure load than other specimens. It is worth noting that the first ply failure load is 2.1 times the buckling load on an average for all the specimens.

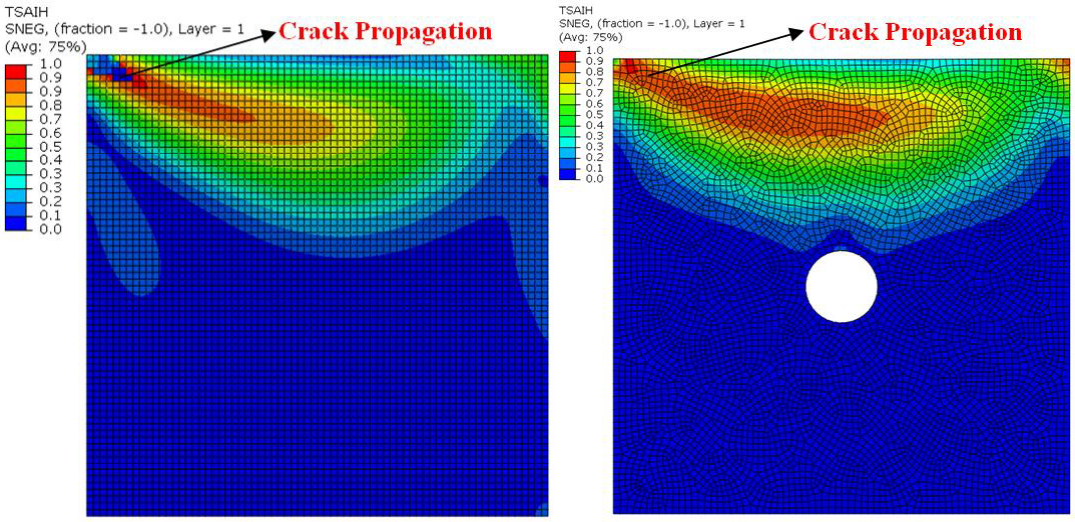

(a) (b)

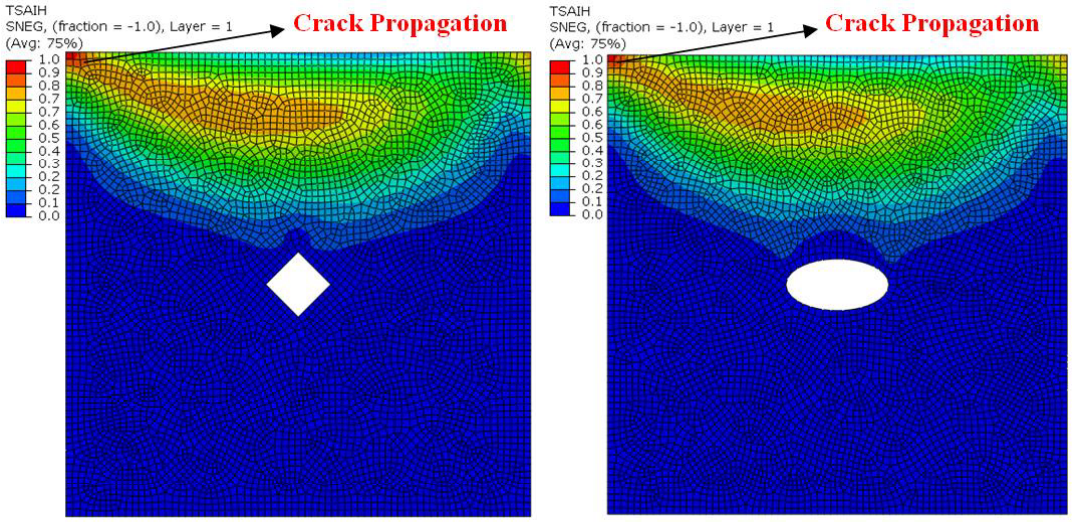

(c) (d)

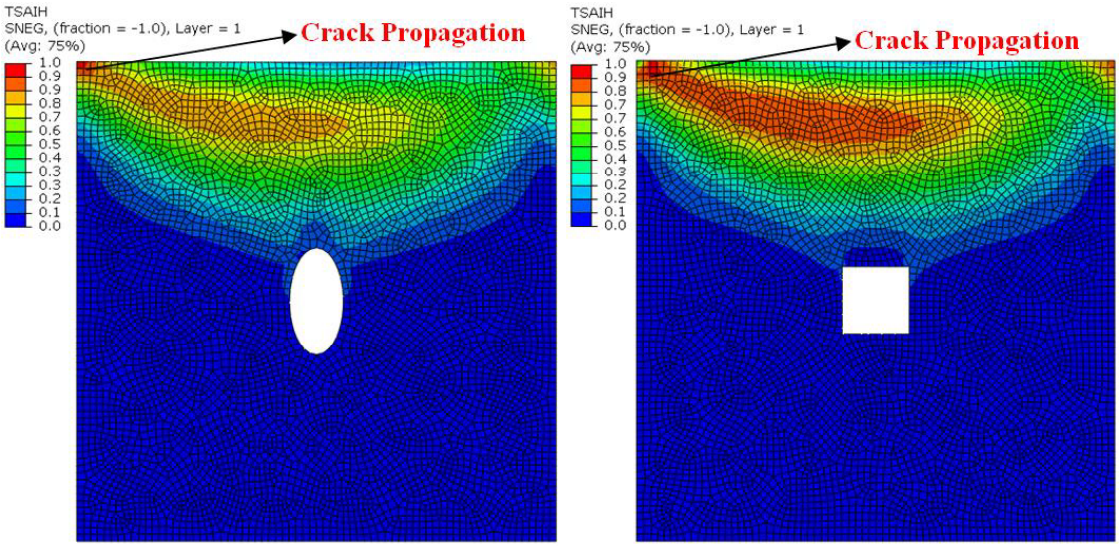

(e) (f)

Fig. 4.16. Initial crack propagation observed in functionally graded composite plates with and without cutouts with fiber aligned in (-45/+45/0/90) direction. The corresponding first ply failure loads (in kN) are given in parenthesis: (a) FH_CG_NC (9.15) (b) FH_CG_C1 (10.03) (c) FH_CG_D1 (10.73) (d) FH_CG_EH1 (11.51) (e) FH_CG_EV1 (10.40) (f) FH_CG_S1 (10.68)

4.3.3.3. $(-45/+45/0/90)_{2s}$ stacking sequence

The load versus maximum out-of-plane displacement curves of functionally graded hybrid plates with different shaped cutouts of small, medium, and big size and with fiber aligned in $(-45/+45/0/90)_{2s}$ direction are discussed below. Crack propagation occurred in the plates with fiber is aligned in $(-45/+45/0/90)_{2s}$ direction is shown in Fig. 4.16 in which Fig. 4.16(a) depicts the plate without cutout. Figs. 4.16(b), 4.16(c), 4.16(d), 4.16(e), and 4.16(f) show the plates with different shaped cutouts such as circle, diamond, ellipse-horizontal, ellipse-vertical, and square cutouts, respectively. The crack propagation in these plates are similar to the plates stacked in $(-45/+45)_{4s}$ direction. But in plates with stacking sequence of $(+45/-45/0/90)_{2s}$, failure loads are higher compare to other two plates in which fiber aligned in $(0/90)_{4s}$ and $(-45/+45)_{4s}$ direction. The corresponding first ply failure loads are shown in Fig. 4.17(a) and Table 4.7.

4.3.3.3.1. Small size cutouts

In Fig. 4.17(a), load vs. out-of-plane displacement responses of carbon fiber surfaced functionally graded hybrid composite plates having $(-45/+45/0/90)_{2s}$ stacking sequence can be observed from which it is clear that buckling and first ply failure load trend is similar to that of $(0/90)_{4s}$ stacking sequence. However, CG_FH_EH1_$(-45/+45/0/90)_{2s}$ plate has better performance than plates with

other shaped cutouts. Circular, diamond, ellipse-vertical, and square shaped cutouts has 2%, 0.44%, 3.78%, and 2% lower buckling loads, respectively compared to the plate i.e., CG_FH_EH1_$(-45/+45/0/90)_{2s}$. The first ply failure load is about 2.5 times and ultimate failure load is about three times the buckling load in this category of plates.

4.3.3.3.2. Medium size cutouts

The buckling and first ply failure load of functionally graded carbon surfaced plates with medium sized cutouts are depicted in Fig. 4.17(b). CG_FH_EH2_$(-45/+45/0/90)_{2s}$ specimen has the highest buckling load amongst all medium sized cutout with $(-45/+45/0/90)_{2s}$ stacking sequence as shown in Fig. 4.17(b). Peak first ply failure load can also be observed for composite plate with elliptical shaped cutout aligned horizontally and is almost equal to that of composite plate with square shaped cutout. Maximum buckling load of CG_FH_EH2_$(0/90)_{4s}$ specimen is 6.60%, 2.50%, 11.16%, and 4.55% higher with respect to the plates with circular, diamond, ellipse-vertical, and square shaped cutouts, respectively. It is worth noting that the first ply failure is approximately 2.4 times the buckling load.

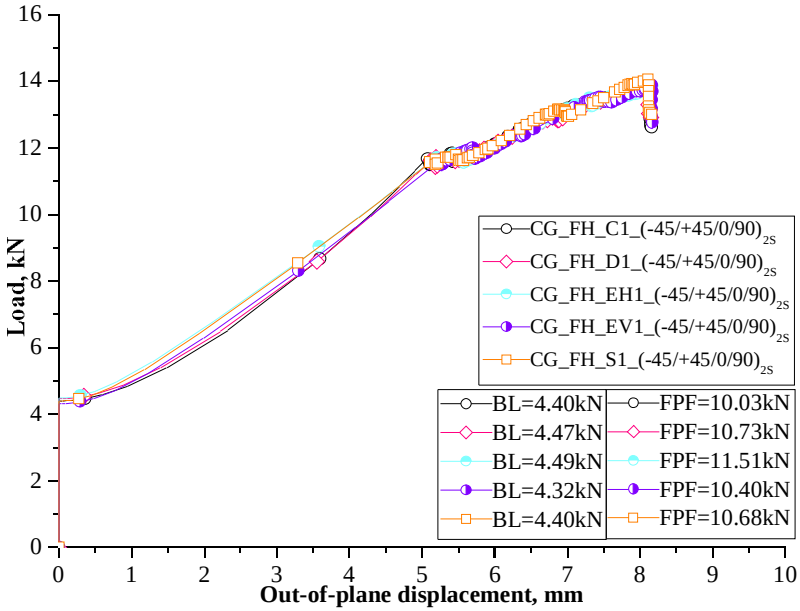

(a)

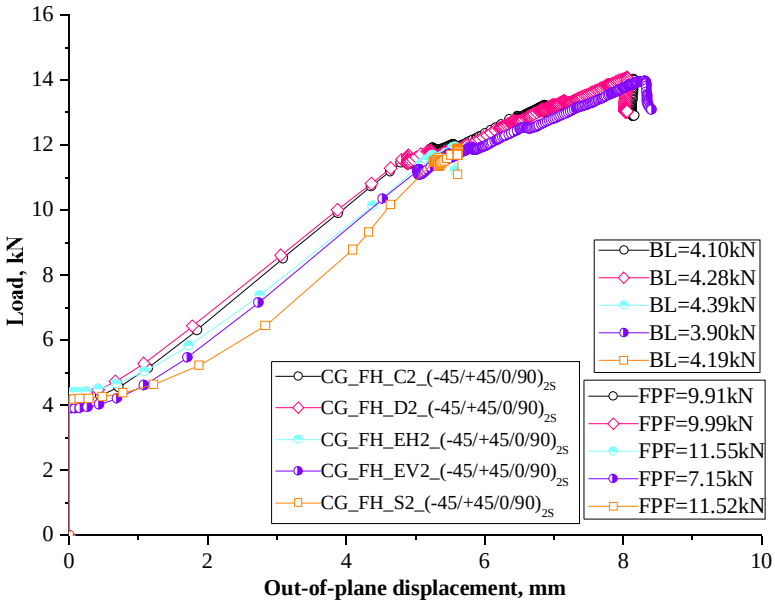

(b)

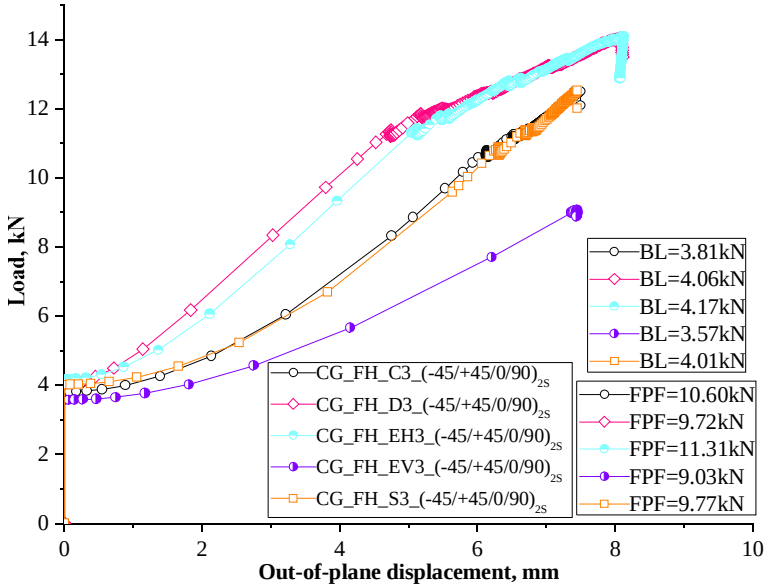

(c)

Fig. 4.17. Load vs. displacement responses of functionally graded hybrid plates with various shaped and sized cutouts stacked in $(-45/+45/0/90)_{2s}$ fiber direction: (a) Small size cutout (b) Medium size cutout (c) Big size cutout

4.3.3.3.3. Big size cutouts

The load vs. displacement responses of functionally graded composite plates with big sized cutouts are shown in Fig. 4.17(c). Peak buckling load and first ply failure load can be observed for

CG_FH_EH3_$(-45/+45/0/90)_{2s}$ plate which has 8.63%, 2.63%, 14.38%, and 3.83% higher buckling load values with respect to plate with circular, diamond, ellipse-vertical, and square shaped cutout, respectively as shown in Fig. 4.17(c). It is worth noting that the first ply failure of the functionally graded composite plates with big size cutouts is approximately 2.6 times the buckling load on an average for all the plates.

4.4. Concluding remarks

In this study, the experimental and numerical investigations have been performed on the plain FRP and hybrid plates with various fiber stacking sequences with simply supported boundary conditions. The numerical results are validated with experimental test results. Further, a parametric study has been performed numerically with the functionally graded composite plates with cutouts of different shapes and sizes. The following concluding remarks are made from this study.

1. Among the composite plates tested experimentally, CFRP plates has better performance in terms of buckling load due to their high material stiffness while GFRP plates ended up with lower buckling load due to their low material stiffness compared to CFRP plates.
2. The out-of-plane displacements are high on an average in case of GFRP plates as well as glass fiber surfaced hybrid plates such as functionally graded and sandwich hybrid due to their lower stiffnesses.
3. The buckling loads obtained from experimental and numerical studies are in good agreement.
4. Among the hybrid plates, functionally graded hybrid plates have higher buckling, first ply failure, and ultimate failure loads when compared with the sandwich hybrid plates. The FH plates with stacking sequence of $(-45/+45/0/90)_{2s}$ outperformed other fiber stacking sequences as far as buckling and first ply failure loads are concerned.
5. Amongst functionally graded composite plates analyzed with various sized cutouts, plates with smaller size cutouts have higher buckling and first ply failure loads. Hence, usage of smaller size cutouts in the composite plates is recommended for practical purposes.
6. From the experiment and numerical studies, it is shown that the hybrid and non-hybrid composite plates can withstand the loads of about four times the buckling loads and about 2.5 times the first ply failure load on an average of all the specimens.

7. The carbon surfaced functionally graded hybrid composite plates with elliptical cutout (aligned horizontally) at the center stacked in $(-45/+45/0/90)_{2s}$ sequence have the highest buckling, first ply failure, and ultimate failure loads.
8. The functionally graded composite plates with elliptical cutout aligned vertically have the lowest buckling loads in all the plates with various shaped and sized cutouts.
9. The functionally graded hybrid composite plates aligned with $(-45/+45/0/90)_{2s}$ stacking sequence are highly recommended through this study to use in practical applications especially where the thin walled structures are subjected to uniaxial compressive loads.